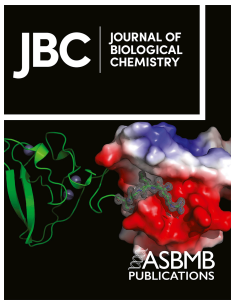

Lysyl hydroxylase 3 mediated post-translational modifications are required for proper biosynthesis of collagen α1α1α2(IV)

Yoshihiro Ishikawa, Yuki Taga, Thibault Coste, Sara F. Tufa, Douglas R. Keene, Kazunori Mizuno, Elisabeth Tournier-Lasserve, Douglas B. Gould

PII: S0021-9258(22)01156-5

DOI: https://doi.org/10.1016/j.jbc.2022.102713

Reference: JBC 102713

To appear in: *Journal of Biological Chemistry*

Received Date: 8 July 2022

Revised Date: 5 November 2022

Accepted Date: 9 November 2022

Please cite this article as: Ishikawa Y, Taga Y, Coste T, Tufa SF, Keene DR, Mizuno K, Tournier-Lasserve E, Gould DB, Lysyl hydroxylase 3 mediated post-translational modifications are required for proper biosynthesis of collagen α1α1α2(IV), *Journal of Biological Chemistry* (2022), doi: https://doi.org/10.1016/j.jbc.2022.102713.

Lysyl hydroxylase 3 mediated post-translational modifications are required for proper biosynthesis of collagen α1α1α2(IV)

Yoshihiro Ishikawa[1]*, Yuki Taga[2], Thibault Coste[3], Sara F. Tufa[4], Douglas R. Keene[4], Kazunori Mizuno[2], Elisabeth Tournier-Lasserve[3] and Douglas B. Gould[1,5]*

From 1 Department of Ophthalmology, University of California San Francisco, School of Medicine, California, USA, 2 Nippi Research Institute of Biomatrix, Ibaraki, Japan, 3 Université Paris Cité, Inserm Neurodiderot, AP-HP Paris, France, 4 Research Department, Shriners Hospital for Children, Portland, Oregon, USA, 5 Department Anatomy, Cardiovascular Research Institute, Bakar Aging Research Institute, and Institute for Human Genetics, University of California, San Francisco, California, USA

*For correspondence: Yoshihiro Ishikawa (yoshihiro.ishikawa@uscf.edu) and Douglas Gould (douglas.gould@ucsf.edu)

Running title: LH3 plays critical roles in type IV collagen biosynthesis

Keywords: collagen, post-translational modification (PTM), hydroxylase, glycosylation, basement membrane

Abstract

Collagens are the most abundant proteins in the body and among the most biosynthetically complex. A molecular ensemble of over 20 endoplasmic reticulum resident proteins participates in collagen biosynthesis and contributes to heterogeneous post-translational modifications. Pathogenic variants in genes encoding collagens cause connective tissue disorders, including Osteogenesis Imperfecta, Ehlers-Danlos syndrome, and Gould syndrome (caused by mutations in *COL4A1* and *COL4A2*), and pathogenic variants in genes encoding proteins required for collagen biosynthesis can cause similar but overlapping clinical phenotypes. Notably, pathogenic variants in lysyl hydroxylase 3 (LH3) cause a multisystem connective tissue disorder that exhibits pathophysiological features of collagen-related disorders. LH3 is a multifunctional collagen modifying enzyme, however its precise role(s) and substrate-specificity during collagen biosynthesis has not been defined. To address this critical gap in knowledge, we generated LH3 knockout cells and performed detailed quantitative and molecular analyses of collagen substrates. We found that LH3 deficiency severely impaired secretion of collagen α1α1α2(IV), but not collagens α1α1α2(I) or α1α1α1(III). Amino acid analysis revealed that LH3 is a selective lysyl hydroxylase for collagen α1α1α2(IV) but a general glucosyltransferase for collagens α1α1α2(IV), α1α1α2(I), and α1α1α1(III). Importantly, we identified rare variants that are predicted to be pathogenic in the gene encoding LH3 in two out of 113 fetuses with intracranial hemorrhage – a cardinal feature of Gould syndrome. Collectively, our findings highlight a critical role of LH3 in α1α1α2(IV) biosynthesis and suggest that LH3 pathogenic variants might contribute to Gould syndrome.

Introduction

Collagens are the most abundant proteins in the human body and comprise 28 members encoded by 46 genes (1,2). Pathogenic variants in genes encoding collagens cause a wide range of disorders affecting almost all tissues and organs (3,4). Type I, type III, and type V collagens form fibrils contributing to structural frameworks, and pathogenic variants in these collagens cause connective tissue disorders – Osteogenesis Imperfecta (OI) and Ehlers-Danlos syndrome (EDS) – that affect fibril-rich tissues such as bone, skin, and vascular structures (5-10). In contrast, type IV collagens form flexible networks that are present in the basement membranes of all tissues. Pathogenic variants in type IV collagens cause Alport syndrome (*COL4A3*, *COL4A4*, and *COL4A5*) which primarily affects the glomerular basement membrane (11,12) and Gould syndrome (*COL4A1* and *COL4A2*), a congenital multisystem disorder that includes highly variable cerebrovascular disease, pediatric epilepsy, ocular anterior segment dysgenesis, skeletal myopathy, and nephropathy (13-18).

Collagen biosynthesis is a complex and highly orchestrated process that occurs in the endoplasmic reticulum (ER) and is facilitated by a molecular ensemble (19) of over 20 proteins that participate in four major steps: post-translational modifications (PTMs) of individual collagen chains, trimer assembly, triple helix formation, and

secretion (19-21). Although most components of the molecular ensemble are shared among collagens, the collagen modifying enzymes differ between collagens (22-24), suggesting sub-type specialization of the molecular ensemble (24,25). Moreover, the molecular ensemble and PTMs for type I collagen, the most extensively characterized collagen, show that the PTM profile is also tissue-specific (24,26). PTMs on the collagen triple helix are classified into three types of primary modifications to prolyl or lysyl residues and two types of secondary modifications to hydroxylysines. Prolyl modifications include 4-hydroxyproline (4Hyp) and 3-hydroxyproline (3Hyp) that are generated by prolyl 4 hydroxylases and prolyl 3 hydroxylases, respectively (27). Approximately 40% or more of the prolines are modified to 4Hyp (22,24,28), which provides thermal stability to the collagen triple helix (29-31). In contrast, less than 5% of the prolines are modified to 3Hyp (28,32) which is proposed to mediate protein-protein interactions (32,33). Primary modification of lysine to hydroxylysine is attributed to lysyl hydroxylases (LHs) (27) and secondary modifications of hydroxylysine include two successive and coordinated *O*-glycosylation steps. Hydroxylysine is required for subsequent galactose attachment to make galactosyl hydroxylysines which are further modified by glucose attachment to make glucosyl galactosyl hydroxylysine. This sequence of modifications from lysine, to hydroxylysine, to galactosyl hydroxylysine and glucosyl galactosyl hydroxylysine occurs in the ER during collagen biosynthesis (34,35).

In the case of OI and EDS, it is well documented that pathogenic variations in genes encoding collagens and genes encoding proteins required for collagen biosynthesis lead to similar clinical outcomes (5-10). A similar paradigm may also exist for Gould syndrome as pathogenic variants in glycosyltransferase 25 domain containing 1 (GLT25D1), encoded by collagen β (1-O) galactosyltransferase 1 (*COLGALT1*) cause musculoskeletal (36) and cerebrovascular (37,38) manifestations similar to those observed in individuals with *COL4A1* and *COL4A2* pathogenic variants. Notably, because molecular ensemble proteins can be multifunctional and employed across diverse collagen types, pathogenic variants in encoding genes often cause phenotypes that blend across different clinical categories. An example being LH3, encoded by procollagen-lysine, 2-oxoglutarate 5-dioxygenase 3 (*PLOD3*), whereby pathogenic variants cause connective tissue phenotypes that overlap with Stickler-like syndrome and Epidermolysis Bullosa (39-42). Indeed, clinical features of patients with biallelic loss of function *PLOD3* variants include craniofacial dysmorphisms, skeletal and ocular disorders, sensorineural hearing loss, and variable skin manifestations. Interestingly, in addition to clinical manifestations overlapping Stickler-like syndrome and Epidermolysis Bullosa, cerebral hemorrhages have been reported in three cases with *PLOD3* variants (39,43). LH3 is proposed to have substrate preference for heavily glycosylated collagens (47,50,51) such as type IV collagen (28,32), raising the possibility that *PLOD3* pathogenic variants could also cause Gould syndrome. Supporting this, *Plod3* deficiency in the mouse lead to basement membrane disruptions caused by intracellular accumulation and impaired secretion of type IV collagen that had lower molecular mass suggesting incomplete PTMs (50). Importantly, according to the peptide-based in *vitro* enzymatic analyses, LH3 is striking in that it is a multifunctional enzyme that can execute all the enzymatic roles required for fully modifying lysine to glucosyl galactosyl hydroxylysine – lysyl hydroxylase, galactosyltransferase, and glucosyltransferase (39,44-49). However, detailed quantitative PTM analysis has never been conducted for any type of collagen in the context of LH3 deficiency. Thus, in this study, we used CRISPR-mediated gene editing to knockout (KO) LH3 both in PFHR9 cells and mouse embryonic fibroblasts (MEFs) and performed a multifaceted investigation including cellular biochemistry, structural assessment, and quantitative PTM characterization for collagen $\alpha1\alpha1\alpha2$(I), $\alpha1\alpha1\alpha1$(III), and $\alpha1\alpha1\alpha2$(IV) to elucidate the role of LH3 in the collagen molecular ensemble. Furthermore, since perinatal cerebral hemorrhage is a cardinal feature of Gould syndrome, we performed a genetic screen for *PLOD3* variants in a fetal stroke cohort that was negative for *COL4A1* and *COL4A2* pathogenic variants.

Results

LH3 is required for secretion of collagen α1α1α2(IV), but not collagens α1α1α2(I) or α1α1α1(III). To explore the role of LH3 in the molecular ensemble for type IV collagen, we used CRISPR-mediated gene editing to knockout (KO) LH3 in PFHR9 cells (Figure 1A and Figures S1 and S2A). We selected PFHR9 cells because they are well characterized and secrete large amounts of collagen $\alpha1\alpha1\alpha2$(IV) due to a duplication of the *Col4a1/Col4a2* locus (28,32,52). Western blot analysis revealed a significant reduction in COL4A1 and COL4A2 protein levels in the conditioned culture medium of LH3 KO PFHR9 cells (Figure 1B and Figure S2B) and a concomitant increase in intracellular COL4A1 protein levels (Figure 1C and Figure S2C), indicating that LH3 deficiency impairs collagen $\alpha1\alpha1\alpha2$(IV) secretion. To quantitively evaluate the effect of LH3 KO on collagen

α1α1α2(IV) biosynthesis we tested the rate of secretion using pulse chase labeling with the methionine analog L-azidohomoalanine (AHA) (53,54). Although this approach is well established for collagen α1α1α2(I), precise measurements of collagen α1α1α2(IV) secretion have not been carefully determined (55-58). AHA pulse chase analysis in wild-type (WT) PFHR9 cells showed that newly synthesized collagen α1α1α2(IV) takes approximately 7 – 8 hours to be secreted (Figure 1D, Table S1, and Figure S3) compared to approximately 2 hours for collagen α1α1α2(I) (59,60). However, in LH3 KO PFHR9 cells, collagen α1α1α2(IV) secretion was significantly delayed and only one-fourth of newly synthesized collagen α1α1α2(IV) was secreted even after 48 hours in culture (Figure 1E and Table S1).

Because PFHR9 cells produce very low levels of fibrillar collagens, we also used CRISPR-mediated gene editing to knockout LH3 in MEFs to test the effect of LH3 deficiency on collagen α1α1α2(I) and collagen α1α1α1(III) biosynthesis (Figure 2A and Figures S4 and S5A). Notably, Western blot analysis showed that the levels of extracellular collagen α1α1α2(I) were increased in LH3 KO MEFs compared to their WT controls (Figure 2B and Figure S5B). Since the signals of α2(I) chain was stronger than that of α1(I) chain in Western blot (Figure 2B and Figure S5B), we quantitively tested the effect of LH3 KO on collagen secretion rates in MEFs. AHA pulse chase labeling showed that the secretion rates of fibrillar collagens α1α1α2(I) and α1α1α1(III) were comparable between WT and LH3 KO MEFs, although delays were observed at early time points for collagen α1α1α2(I) (Figure 2C and D, Table S2 and Figure S6). Collectively, these data suggest that LH3 is critical for biosynthesis of collagen α1α1α2(IV) but not collagens α1α1α2(I) and α1α1α1(III).

LH3 is required for collagen α1α1α2(IV) to form triple helices and higher-order oligomeric structures. To molecularly characterize the effects of LH3 deficiency on collagens, we purified collagens α1α1α2(I) and α1α1α1(III), and collagen α1α1α2(IV) from the conditioned culture medium of MEFs and PFHR9 cells, respectively (Figure S7A and S7B). Consistent with the Western blot and AHA pulse chase data, there was no difference between collagens α1α1α2(I) and α1α1α1(III) produced by WT and LH3 KO MEFs (Figure 3A). In contrast, collagen α1α1α2(IV) from LH3 KO PFHR9 cells did not show the higher-order collagen α1α1α2(IV) structures that were observed in collagen α1α1α2(IV) from WT PFHR9 cells suggesting an absence of collagen α1α1α2(IV) disulfide cross linking (Figure S7B). We next used SDS-Agarose gel electrophoresis to resolve the oligomeric state of collagen α1α1α2(IV). Consistent with previous reports (52,56), the protein banding pattern observed in WT PFHR9 cells showed that most collagen α1α1α2(IV) was present as trimers or dodecamers unless denatured under reducing conditions when they were resolved as monomers (Figure 3B). In contrast, most of the collagen α1α1α2(IV) isolated from LH3 KO PFHR9 cells was monomeric and failed to form higher order structures (Figure 3B). Interestingly, we detected a lower molecular weight band in the samples isolated from LH3 KO PFHR9 cells on both SDS-Agarose and SDS-PAGE gels (Figure 3B and Figure S7C) that was identified as truncated COL4A1 and COL4A2 proteins by liquid chromatography–mass spectrometry (LC-MS) analysis (Figure S7D). To better characterize collagen α1α1α2(IV) oligomeric structures and network formation, we performed rotary shadow electron microscopy on samples isolated from WT and LH3 KO PFHR9 cells. During type IV collagen network formation, two collagen α1α1α2(IV) heterotrimers associate with each other by way of head-to-head interactions of their carboxy terminal NC1 domains (hexamers) (61) and four collagen α1α1α2(IV) heterotrimers interact by way of lateral, anti-parallel interactions of their amino terminal 7S domains (dodecamers) (62). Electron micrographs from WT PFHR9 cells showed that over 80% of the collagen α1α1α2(IV) was trimeric, but we also found frequent examples of hexamers (~8.5%) and dodecamers (~9.0% (Figure 3C). In contrast, we found reduced proportions of normal trimers and hexamers and did not observe dodecamers in samples from LH3 KO cells. Instead we detected shortened versions of collagen α1α1α2(IV) hexamers (7.8%) and trimers that appeared truncated at the amino termini and corroborate the SDS-gel electrophoreses and LC-MS data (72.8 %) (Figure 3B and 3C and Figure S7B, S7C and S7D).

To evaluate the secondary structure of the collagen α1α1α2(IV) triple helix, we measured circular dichroism (CD) spectra of collagen purified from WT or LH3 KO PFHR9 cells (Figure 3D). At 10 ºC, collagen α1α1α2(IV) isolated from WT cells showed the characteristic triple helical spectra with negative and positive peaks at 200

and 220 nm, respectively (63), and these peaks were lost following heat denaturation at 65 ºC. In contrast, even at 10 ºC collagen α1α1α2(IV) isolated from LH3 KO PFHR9 cells resembled denatured WT collagen α1α1α2(IV) indicating that collagen α1α1α2(IV) produced by LH3 KO cells did not form stable triple helical helices. The triple helical structure is required for binding of the collagen molecular chaperone HSP47 (64) which plays a critical role in collagen trafficking by anchoring collagens to TANGO1 at ER exit sites to continue along the secretory pathway to the Golgi (65). To test whether HSP47 could bind purified collagen α1α1α2(IV), we performed surface plasmon resonance (SPR) analysis. HSP47 interacted with immobilized collagen α1α1α2(IV) from WT PFRH9 cells in a concentration dependent manner (Figure 3E). Although HSP47 also interacted with collagen α1α1α2(IV) from LH3 KO PFRH9 cells, the binding kinetics were altered with lower binding affinity and increased dissociation constant.

LH3 is a selective lysyl hydroxylase but a general collagen glucosyltransferase. PTMs are important for the structural integrity of collagen triple helices. To understand how LH3 deficiency impacted collagen PTMs, we quantified prolyl hydroxylation, lysyl hydroxylation, and *O*-glycosylated hydroxylysine using amino acid analyses (AAA) combined with LC-MS. First, we performed acid hydrolysis AAA (which removes sugar groups) of individual collagen α chains from WT or LH3 KO cells. We found that prolyl 3 hydroxylation, which occurs infrequently, was largely unchanged by LH3 deficiency across COL1A1, COL1A2, COL3A1, COL4A1, and COL4A2 proteins and that prolyl 4 hydroxylation was reduced for COL4A1, but not for the other α chains (Figure 4A and Table S3). In contrast, we found more unmodified lysines (significantly fewer hydroxylysines), on COL4A1 and COL4A2 proteins isolated from LH3 KO PFHR9 cells compared to WT PFHR9 cells. The levels of lysine/hydroxylysine for COL1A1, COL1A2, and COL3A1 isolated from MEFs were largely unchanged, suggesting that the lysyl hydroxylase function of LH3 is selective for collagen α1α1α2(IV) (Figure 4A and Table S3). Next, we used alkaline hydrolysis AAA (which preserves sugar attachments) combined with LC-MS to compare the extent of galactosyl hydroxylysine and glucosyl galactosyl hydroxylysine on collagens between WT and LH3 KO cells. Type IV collagen is highly glycosylated and hydroxylysine residues from collagen α1α1α2(IV) produced by WT PFHR9 cells were almost fully modified to glucosyl galactosyl hydroxylysine (Figure 4B and Figure S8). In contrast, collagen α1α1α2(IV) derived from LH3 KO PFHR9 cells had high occupancy of galactosyl hydroxylysine but not glucosyl galactosyl hydroxylysine suggesting that in addition to its role as a lysyl hydroxylase, LH3 also participates in glucosyl, but not galactosyl, modifications. As reported previously (47,66), glucosyl galactosyl hydroxylysine was also reduced in collagens α1α1α2(I) and collagen α1α1α1(III) suggesting that LH3 is also involved in glucosyl modifications of fibrillar collagens (Figure 4B and Figure S8). Taken together, these data suggest that LH3 has selective lysyl hydroxylase activity but general collagen glucosyltransferase activity.

Rare PLOD3 variants in fetuses with intracerebral hemorrhage. The role for LH3 in collagen α1α1α2(I) and collagen α1α1α1(III) glycosylation is consistent with the identification of *PLOD3* pathogenic variants in individuals with connective tissue disorders (39,41). However, our data demonstrate that LH3 plays an even greater role in collagen α1α1α2(IV) biosynthesis. Consistent with this finding, *Plod3* deficiency in the mouse caused basement membrane defects (47,50), suggesting that *PLOD3* pathogenic variants may also contribute to intracerebral hemorrhages (ICHs) which constitute a central pathophysiological hallmark of Gould syndrome caused by *COL4A1* and *COL4A2* pathogenic variants (13-15,67-71). In addition, cerebrovascular hemorrhages have been reported in three patients with a connective tissue disorder caused by biallelic pathogenic variants of *PLOD3* (39,43). To investigate the potential involvement of *PLOD3* in ICH, we specifically evaluated the presence of *PLOD3* variants in exome sequencing data from a fetal ICH cohort consisting of 113 probands who did not have *COL4A1* or *COL4A2* pathogenic variants. We did not find an enrichment of rare and predicted damaging *PLOD3* qualifying variants between this cohort and the gnomAD control database (Table 1). However, in two unrelated fetuses, we identified three rare (<1/1000) *PLOD3* missense variants – all three were predicted to be damaging by PolyPhen-2 (Figure 5A and Table 2). Fetus F09 was heterozygous for p.L198P variant and fetus F12 was compound heterozygous for p.R197W and p.P489L. Variants p.R197W and p.L198P are located in the catalytic glycosyltransferase domain close to a poly Asp sequence and predicted to affect the overall structure of active site in the transferase domain (48) (Figure 5B). The p.P489L variant is located in the accessory

glycosyltransferase domain and predicted to affect the substrate recognition (Figure 5B). The two fetuses with predicted pathogenic variants had ICH identified on ultrasound follow up during the third trimester of pregnancy. Upon cerebral imaging, they presented a bilateral ventriculomegaly and intraparenchymal lesions (Table 3). Due to the severity of these lesions, the parents opted for termination of pregnancy. The lesions were confirmed by postmortem examination, and the fetuses showed some phenotypic differences. The fetus F12 had intraparenchymal hemorrhagic and ischemic lesions, whereas the fetus F09 had a microcephaly, a very thin corpus callosum and a white matter atrophy. Neither had bone abnormalities or signs of external visceral malformation.

Discussion

To clarify the role(s) for LH3 in collagen biosynthesis, we generated LH3 KO cells using CRIPSR- mediated gene editing to conduct detailed quantitative and molecular analyses of collagens α1α1α2(I), α1α1α1(III) and α1α1α2(IV) implicated in OI, EDS and Gould syndrome, respectively. We discovered that LH3 deficiency severely impaired biosynthesis of collagen α1α1α2(IV), but not collagens α1α1α2(I) or α1α1α1(III). Our findings revealed altered PTMs in collagen α1α1α2(IV) produced by LH3 KO PFHR9 cells characterized by reduced and impaired modification of lysine to hydroxylysine and galactosyl hydroxylysine to glucosyl galactosyl hydroxylysine. These PTM alterations prevented proper heterotrimer formation and HSP47 binding which impaired collagen α1α1α2(IV) secretion. Notably, collagen α1α1α2(IV) that was secreted from LH3 KO PFHR9 cells showed impaired collagen α1α1α2(IV) network formation and failed to make higher order oligomers. In contrast, LH3 deficiency did not impact primary modifications to prolyl and lysyl residues for collagens α1α1α2(I) and α1α1α1(III) but specifically reduced modification of galactosyl hydroxylysine to glucosyl galactosyl hydroxylysine. Thus, we suggest that LH3 may be a selective lysyl hydroxylase at least for collagen α1α1α2(IV) and that network-forming and fibrillar collagens are both important substrates for LH3 glucosyltransferase activity.

Our results indicate that LH3 plays a critical role for collagen α1α1α2(IV) biosynthesis in PFHR9 cells but not for collagens α1α1α2(I) and α1α1α1(III) in MEFs. Surprisingly, Western blot analysis for PFHR9 cells showed that protein levels of intracellular COL4A2 in KO cells were similar to WT control cells, however the protein migrated slightly faster and its secretion was significantly impaired (Figure 1B and 1C), indicating there could be a different quality control mechanism between COL4A1 and COL4A2 proteins. Although the majority of synthesized collagen α1α1α2(IV) was accumulated intracellularly in LH3 KO PFHR9 cells, some collagen α1α1α2(IV) was successfully secreted but did not have stable triple helical structures. Based on the current understanding of fibrillar collagen biosynthesis, this finding is intriguing for two reasons. First, the amount of 4Hyp is essential to the formation of triple helix rigidity (29). Type II collagen containing approximately 30% 4Hyp from *P4ha1*$^{+/-}$, *P4ha2*$^{-/-}$ mice (*P4ha1* and *P4ha2* encoded prolyl 4-hydroxylase 1 and 2, respectively) decreased its thermal stability compared to a WT control, however this type II collagen remained capable of forming a triple helical structure (72). Notably, the COL4A1 produced by LH3 KO PFHR cells showed a reduction of 4Hyp (Figure 4A) but still contained around total 45 % 4Hyp in the collagen α1α1α2(IV) heterotrimer isolated from LH3 KO PFHR9 cells, which is calculated by the amount of 4Hyp in COL4A1 and COL4A2 (TableS3). Second, the amounts of hydroxylysine do not affect triple helix formation. Collagen α1α1α2(I) containing only 1.5 % hydroxylysine can form fully rigid triple helices and secrete into the extracellular matrix properly (24). Also, increased hydroxylysines in collagen α1α1α2(I) do not improve collagen thermal stability (73). Based on these observations, it is tempting to speculate that lysyl hydroxylation and/or the subsequent *O*-glycosylation critically contributes triple helix stability in collagen α1α1α2(IV).

Interestingly, the AHA pulse-chase experiments showed that the secretion rate of collagen α1α1α2(IV) was remarkably slower than that of collagens α1α1α2(I) and α1α1α1(III) (Figure 1D and 2D). A significant difference between collagen α1α1α2(IV) and fibrillar collagens (type I, II, III and V) is the presence of multiple interruptions of the collagenous repeats which occur more frequently nearer the amino terminus (74). Repeat interruptions, which would be pathogenic if they occurred in fibrillar collagens, may interfere with propagation of triple helix formation, requiring re-nucleation of the three alpha chains, and likely contribute to the much longer secretion

time for collagen α1α1α2(IV) compared to collagens α1α1α2(I) and α1α1α1(III). We hypothesize that the complement of PTMs near repeat interruptions may provide thermal or structural stability required for re-nucleation and propagation of the collagen α1α1α2(IV) triple helix. Supporting this notion, collagen α1α1α2(IV) from LH3 KO cells appeared shorted on rotary shadow images, which may suggest the amino termini are disordered and cannot be resolved by electron microscopy. Alternatively, they may be more susceptible to cleavage, leading to a truncated protein of lower molecular weight as demonstrated by SDS gel electrophoreses and LC-MS analysis (Figure 3B and 3C and Figure S7B, S7C and S7D). Structural alterations of the 7S domain at the amino termini could be responsible for the inability to form higher order dodecamer structures in collagen α1α1α2(IV) isolated from LH3 KO PFHR9 cells (Figure 3B and 3C and Figure S7B, S7C and S7D). While the CD spectra showed that the overall secondary structure of collagen α1α1α2(IV) produced by LH3 KO was not fully triple helical (Figure3D), HSP47 was still able to bind with this collagen α1α1α2(IV). We speculate that this binding occurs on the triple helical carboxyl terminus region and weakly associate with the immature amino terminus gelatin-like structure (Figure 3E). Interestingly, small amounts of collagen α1α1α2(IV) were secreted from LH3 KO cells without a robust triple helical structure, which raises the question: what are the essential chemical or structural factors for collagen α1α1α2(IV) triple helix formation and for passing through quality control checkpoints in the ER and secretory pathway? Further experiments are required to provide additional mechanistic insights into the role of PTMs in collagen α1α1α2(IV) biosynthesis, secretion, and function(s).

Since our findings establish a critical role for LH3 in collagen α1α1α2(IV) biosynthesis, we predicted that *PLOD3* might lead to clinical manifestations similar to those observed in individuals with *COL4A1* and *COL4A2* pathogenic variants causing Gould syndrome, a multisystem disorder frequently manifesting as fetal and perinatal ICH (13-15,67-70). Previously identified pathogenic *PLOD3* missense variants cause phenotypically overlapping connective disorders including Stickler-like syndrome and Epidermolysis Bullosa (39-42). In addition to the clinical features encountered in these two conditions, spontaneous ICH has been reported by Salo et al. in two siblings (39). One of them was a female child with a connective tissue disorder, consisting of craniofacial dysmorphism, sensorineural deafness and skeletal features, who presented a spontaneous large brain hematoma. Her male sibling was stillborn at 28 weeks of gestation; in addition to skeletal anomalies, autopsy of this fetus showed porencephaly. DNA analysis showed biallelic *PLOD3* variants (p.N223S/p.C691AfsX9) located in a conserved region of the LH3 amino acid sequence responsible for collagen glycosyltransferase and lysyl hydroxylase activities. Recently, a homozygous *PLOD3* small inframe deletion was shown to cause a cerebral small vessel disease characterized by multiple white matter hypersignals and bleeding foci in an infant with a few dysmorphic features (43). To evaluate the contribution of *PLOD3* pathogenic variants to cerebrovascular manifestations, we analyzed a series of 113 cases of fetal ICH that were negative for *COL4A1* and *COL4A2* pathogenic variants. We identified a rare and predicted damaging heterozygous variant in one fetus (F09) and two distinct biallelic candidate variants in another fetus (F12) (Figure 5 and Table 2). When comparing the whole cohort of fetuses to control databases, we did not detect an enrichment in rare and predicted damaging *PLOD3* variants; however, this lack of enrichment could be attributable to the high genetic heterogeneity of fetal ICH (71). Additional work is required to establish the causality of the heterozygous *PLOD3* variant present in fetus F09. Indeed, connective tissue disorders associated with *PLOD3* are typically autosomal recessive and heterozygous parents of affected cases are reported to be asymptomatic. We cannot exclude however that some heterozygous *PLOD3* variants could have dominant negative effects or that they could act as risk factors acting in concert with other triggering events to cause fetal ICH. For fetus F12, who is a compound heterozygote with both variants being predicted to be possibly pathogenic, no tissue was available to evaluate the consequences of the two variants at the protein level. Autopsy data including skeletal X-Ray data were normal. Additional *in vitro* experiments are required to determine the causality of these variants and larger cohorts of fetuses and children with ICH should be analyzed to identify additional cases.

In conclusion, our results suggest that LH3 plays a critical and multifunctional role in collagen α1α1α2(IV) biosynthesis, and that *PLOD3* variants could lead to clinical manifestations associated with *COL4A1* and *COL4A2* pathogenic variants.

Experimental Procedures

Cell Culture – PFHR9 cells (CRL-2423) and mouse embryonic fibroblasts (MEFs: CRL-1503) were purchased from ATCC. These cells were cultured in DMEM (Dulbecco modified essential medium)/high glucose/pyruvate (Gibco: 11995065) supplemented with 10% (vol/vol) Fetal Bovine Serum (Atlanta Biologicals), Pen Strep Glutamine 100× (Gibco: 10378016), and 5 mM Hepes in presence of ascorbic acid phosphate (100 µg/mL; Wako Chemicals). After this section, standard DMEM indicates the DMEM above.

CRISPR mediated knockout of LH3 – LH3 was knocked out in PFHR9 cells and MEFs using two CRISPR/Cas9 All-in-One plasmid of pSpCas9(BB)-2A-Puro (PX459) v2.0 and pSpCas9(BB)-2A-GFP (PX458) including the LH3 gRNA sequence for *Plod3* exon 5 (5'- TCCACTGGCGGACAATCTGATGG -3') and exon 7 (5'- TCGTGTGCGCATCCGGAATGTGG -3') which were designed and purchased from GenScript (Piscataway, NJ), respectively. Two plasmids were transfected into the cells using Lipofectamine 3000 (Life Technologies) according to manufacturer's instructions. After 24 hours, transfected cells were treated with 10 µg/ml puromycin (Gibco) to select cells containing the PX459 plasmid. After puromycin selection, the GFP-positive cells containing the PX458 plasmid were isolated using a corning ring and cultured them with standard DMEM.

DNA sequencing – To confirm LH3 gRNA edited *Plod3* exon 5 and 7, PCR products including the region targeted with gRNA were sequenced. DNA was prepared from WT and LH3 KO cells. Cells were plated onto 6 cm dish and grown to 100 % confluency. Cells were collected by centrifugation after treating with trypsin. This cell pellet was digested by 3 mg/mL proteinase K in 20 µL of 50 mM Tris/HCl buffer containing 20 mM NaCl, 1 % SDS and 1 mM EDTA, pH 8.0 at 95 °C for 5 min after preincubating at 60 °C for 60 min. After the digestion, 200 µL of H_2O was added to this solution as a template for PCR. PCR was performed with primer set A (Fwd: 5'-AAGCGCTTCCTCAACTCTG-3' and Rev: 5'-TCCCTCATTACCCACCTCTAA-3') and B (Fwd: 5'-ACTCCTGAGCATGTGTGTTAG-3' and Rev: 5'-ACAGGGTTGAGTGGCTAAAG-3') for exon 5 and 7, respectively. Sequencing samples including the Fwd primer were sent to Quintara Biosciences (Hayward, CA). Sequencing results were analyzed by GeneStudio™ Professional Edition Version 2.2.0.0 (GeneStudio Inc.)

Protein analyses in cell lysate and conditioned culture medium – WT and LH3 KO cells were plated and grown to 80 – 90 % confluency. Following stimulation of procollagen biosynthesis with ascorbic acid for one day, the medium was replaced to the fresh standard DMEM, and the cells were cultured for two days. The medium containing secreted proteins was dissolved in Bolt LDS sample buffer 4X (Life Technology) with reducing agents. After the cells were washed with PBS once, cell lysates were extracted using M-PER (Thermo Fisher Scientific) containing Halt™ Protease Inhibitor Cocktail, EDTA-Free (Thermo Fisher Scientific) at 4 °C according to manufacturer's instructions. After centrifugation, soluble proteins in the supernatant were mixed with the same sample buffer with reducing agents. These protein solutions were separated on SDS-PAGE gels then transferred to PVDF membranes, and Western blots were performed. Gels, buffers, transfer condition and antibodies are listed in Table S4. Blots were developed with HRP enhanced Super-Signal West Pico Chemiluminescent Substrate (Thermo Fisher Scientific) and detected by ChemiDoc MP imaging system (BioRad) using the software Image Lab version 4.0.1 (BioRad). The intensities of protein signals were measured by Image J.

Secretion rate assay for PFHR9 cells – WT and LH3 KO cells were cultured in a 16 cm dish grown to 100 % confluency and equally plated to three 6-well tissue culture plates after the cells were trypsinized. Following stimulation of procollagen biosynthesis with ascorbic acid overnight, the cells were preincubated in pulse medium (Met- and Cys-free DMEM with 10% FBS and 100 µg/ml ascorbic acid 2-phosphate) without L-azidohomoalanine (AHA, Click Chemistry Tools) at 37 °C for 30 min to deplete methionine. Pulse labeling was performed with 1 mM AHA in pulse medium at 37 °C for 15 min, and cells were incubated in 1.5 mL chase medium (standard DMEM) at 37 °C for different time intervals (*i.e*. every 30 min by 360 min, 420 min 480 min, 24 h and 48 h). The conditioned culture medium was collected at each time point and frozen at -20 °C. After thawing and centrifuging at high speed to remove residual cells and large aggregates, 1.4 mL of medium was mixed with 1.4 mL of 0.1 M Tris/HCl containing 1.0 M urea, pH7.5. This solution was incubated 0.4 mL of Q sepharose Fast Flow (GE

Healthcare) to remove AHA incorporated laminins at room temperature for an hour. After centrifugation at high speed for 10 min, 2.8 mL supernatant was mixed with 0.2 mL 10 M acetic acid and 1 mL of 5 M NaCl at 4 °C overnight. Collagen α1α1α2(IV) was precipitated at the highest speed by a tabletop centrifuge. The pellet containing collagen α1α1α2(IV) was dissolved in 27 µL of TBS and labeled with 3 µL of Click-iT Alexa Fluor 488 sDIBO Alkyne (Thermo Scientific) at room temperature for an hour. In LH3 KO secretion rate assay, the pellets from 2-well in the 6-well plate were combined to detect adequate signals. This labeled solution was mixed with 10 µL of 4x Bolt LDS Sample Buffer with reducing agent and separated on precast 6 % Tris/Glycine gel (Invitrogen). The signals from AHA-Alexa Fluor 488 were detected by the ChemiDoc MP imaging system (BioRad) using the software Image Lab version 4.0.1 (BioRad). The intensities of fluorescent signals were measured by Image J. The AHA incorporated collagen α1α1α2(IV) as a loading control was purified from conditioned culture medium after an hour pulse and the overnight chase. The purification method is described in the section "Collagen α1α1α2(IV) purification" below. This assay was performed 5 times and representative images are shown.

Secretion rate assay for MEFs – WT and LH3 KO cells were cultured in a 16 cm dish grown to 100 % confluency and equally plated to five 10 cm dishes plate after the cells were trypsinized. Following stimulation of procollagen biosynthesis with ascorbic acid overnight, cells were preincubated in pulse medium without AHA at 37 °C for 30 min to deplete methionine. Pulse labeling was performed with 1 mM AHA in pulse medium at 37 °C for 15 min, and cells were incubated in 3.7 mL chase medium (standard DMEM) at 37 °C for different time intervals (*i.e*. every 30 min, 60 min, 90 min, 120 min and 180 min). The conditioned culture medium was collected at each time point and frozen at -20 °C. After thawing and centrifuging at high speed to remove residual cells and large aggregates, 3.5 mL of medium was mixed with 0.5 mL 10 M acetic acid and 20 µL of 100 mg/mL pepsin at 4 °C overnight. After adding 1.0 mL of 5 M NaCl to the pepsin treated solution and incubating at 4 °C overnight, collagens α1α1α2(I) and α1α1α1(III) were precipitated at the highest speed by a tabletop centrifuge. The pellet containing collagens α1α1α2(I) and α1α1α1(III) was dissolved in 27 µL of TBS and labeled with 3 µL of Click-iT Alexa Fluor 488 sDIBO Alkyne (Thermo Scientific) at room temperature for an hour. This labeled solution was mixed with 10 µL of 4x Bolt LDS Sample Buffer without reducing agent and separated on precast 6 % Tris/Glycine gel (Invitrogen). The signals from AHA-Alexa Fluor 488 were detected by the ChemiDoc MP imaging system (BioRad) using the software Image Lab version 4.0.1 (BioRad). The intensities of fluorescent signals were measured by Image J. The AHA incorporated type I and type III collagen as a loading control was purified from conditioned culture medium after an hour pulse and the overnight chase. The purification method is described in the section "Collagens α1α1α2(I) and α1α1α1(III)purification" below. This assay was performed 5 times and representative images are shown.

Collagen α1α1α2(IV) purification – Extraction of collagen α1α1α2(IV) was performed using the standard DMEM with PFHR9 cells. DMEM was prepared by the same procedures as described in "Protein level analyses" above, except using serum free DMEM instead of the standard DMEM. The DMEM was dialyzed with 0.2 M acetic acid at 4 °C overnight. After spinning down to remove residual cells or aggregates, the DMEM was dialyzed with 0.2 M acetic acid containing 1.2 M NaCl at 4 °C overnight. The precipitates including collagen α1α1α2(IV) were collected by centrifugation at 13,000 rpm for 20 min using JA-14 rotor (Beckman) and resuspended with 50 mM Tris/HCl buffer containing 25 mM NaCl and 0.5 M urea, pH 7.5. After dialysis to the same buffer at 4 °C overnight and centrifugation at 13,000 rpm for 10 min using JA-20 rotor (Beckman), the solution was applied to HiTrap Q FF column (cytiva), and the flow through (FT) fraction was collected. The FT was dialyzed to 50 mM MES buffer containing 25 mM NaCl and 0.5 M urea, pH 6.0, at 4 °C overnight and applied to HiTrap SP HP column (cytiva). After washing with the same MES buffer at least five column volumes, collagen α1α1α2(IV) was eluted by 50 mM MES buffer containing 250 mM NaCl and 0.5M urea, pH 6.0. The fractions containing collagen α1α1α2(IV) were concentrated using Amicon Ultra centrifugal filters Ultracel – 100K (Millipore) at the speed x 100 g up to 1.5 mL as a total volume. The concentrated fraction was dialyzed to 0.2 M acetic acid at 4 °C overnight, and 0.5 mL of 5 M NaCl was added (final concentration 1.25 M NaCl) to the dialyzed solution. After mixing at 4 °C overnight, collagen α1α1α2(IV) was precipitated by centrifugation at 14,000 rpm for 20 min using

a tabletop centrifuge. The pellet was resuspended with 0.2 M acetic acid dialyzed to 0.2 M acetic acid at 4 °C overnight to remove residual NaCl for experiments.

Collagens α1α1α2(I) and α1α1α1(III) purification – Extraction of collagens α1α1α2(I) and α1α1α1(III) was performed using the cultured standard DMEM with MEFs. The DMEM was prepared by the same procedures as described in "Protein level analyses" above. The DMEM was dialyzed with 0.5 M acetic acid at 4 °C overnight. After spinning down to remove residual cells or aggregates, the DMEM was incubated with pepsin added to a final concentration of 0.25 mg/ml at 4 °C overnight. The pepsin treated DMEM was dialyzed with 0.5 M acetic acid containing 0.7 M NaCl at 4 °C overnight. The precipitates including collagens α1α1α2(I) and α1α1α1(III) were collected by centrifugation at 13,000 rpm for 20 min using JA-14 rotor (Beckman). The pellet was resuspended in 0.2 M acetic acid and, this solution contained enriched collagens α1α1α2(I) and α1α1α1(III) was dialyzed to 0.2 M acetic acid at 4 °C overnight to remove residual NaCl for experiments.

SDS-gel analyses – To check purity, the isolated collagens were run on a Bolt 4 -12 % Bis-Tris Plus gel (Invitrogen) in the presence or absence of DTT with MES running buffer (Novex) after boiling denaturation. To compare differences in migration, the purified collagens α1α1α2(I) and α1α1α1(III) mixture were run on a 3-8 % Tris/Acetate gel (Invitrogen) in the presence or absence of DTT with boiling denaturation. To demonstrate higher-order collagen α1α1α2(IV) collagen assemblies, SDS-agarose gel electrophoresis was performed for purified WT and LH3 KO collagen α1α1α2(IV). 3.5 % agarose was dissolved in 0.2 M Tris/HCl, pH 8.8. After measuring the total weight of the beaker and agarose solution, the beaker was heated in a microwave oven and gently swirled to thoroughly mix the agarose solution. After adding 20 % SDS up to 0.25 % and sufficient hot distilled water to obtain the initial weight, the SDS-agarose solution was mixed thoroughly again. Bio-Rad Mini-PROTEAN Tetra Handcast Systems was adapted to cast the gel, and hot SDS-agarose solution was loaded between pre-heated glass plates of a vertical electrophoresis apparatus. Four different sample conditions were prepared using purified WT and LH3 KO collagen α1α1α2(IV) in the presence or absence of DTT with and without boiling denaturation. The samples were separated on a SDS – 3.5 % agarose gels with Tris/glycine SDS running buffer using 75 V constant voltage at 4 °C for about 2 hours. All gels were stained with GelCode Blue Stain Reagent (Thermo Scientific). For PTMs analysis, we used 6 % Tris glycine SDS-PAGE and 3.0 % SDS-Agarose gel to separate individual collagen chains of collagens α1α1α2(I) and α1α1α1(III) and collagen α1α1α2(IV) under reducing condition, respectively. After gels were electrophoretically transferred to PVDF membranes with 0.05 % SDS, the membranes were stained with ponceau S.

Protein identification by LC-MS – Gel bands were reduced with 10 mM dithiothreitol at 56 °C for 30 min followed by alkylation with 50 mM iodoacetamide at room temperature for 30 min. The samples were digested with trypsin (Promega, Madison, WI, USA) at 37 °C for 16 h, and the generated tryptic peptides were sequentially extracted from the gels with 5% formic acid, 5% formic acid/50% acetonitrile, and 5% formic acid/95% acetonitrile. The extracted solutions were concentrated by a centrifugal evaporator CVE-3100 (EYELA, Tokyo, Japan) and then analyzed by LC-MS liquid chromatography–mass spectrometry on a maXis II quadrupole time-of-flight mass spectrometer (Bruker Daltonics, Bremen, Germany) coupled to a Shimadzu Prominence UFLC-XR system (Shimadzu, Kyoto, Japan) with chromatographic separation using an Ascentis Express Peptide ES-C18 column (2.7 µm particle size, L × I.D. 150 mm × 2.1 mm; Supelco, Bellefonte, PA, USA) (75). The MS scan and MS/MS acquisition were performed over the *m/z* ranges of 50−2500 with a frequency of 5 Hz. The acquired MS/MS spectra were searched against the UniProtKB/Swiss-Prot database (release 2018_05) for *Mus musculus* species using ProteinPilot software 4.5 (AB Sciex, Foster City, CA, USA), as described previously (24).

Rotary shadow electron microscopy – Rotary shadowing was performed by methods described previously (76). In brief, samples were prepared to mix WT and LH3 KO collagen α1α1α2(IV) (approximate concentrations of 100 µg/ml) in 0.2 M acetic acid with glycerol to a final concentration of 70% glycerol. Each protein was nebulized onto freshly cleaved mica chips using an airbrush. The samples were then rotary shadowed with carbon/platinum using an electron beam gun within a vacuum evaporator. Images were acquired using a FEI

G20 transmission electron microscope. Proportions of different heterotrimer structures were obtained from images of WT (n = 690) and LH3 KO (n = 295) molecules and representative images were used in Figure 4C.

Circular dichroism – CD spectra were recorded on an AVIV 202 spectropolarimeter (AVIV Biomedical, Inc) using a Peltier thermostat-controlled cell holder and a 1 mm path length rectangular quartz cell (Starna Cells Inc). Protein concentrations were determined by acid hydrolysis amino acid analysis described in the section "PTMs analysis by LC-MS" and using collagen solution instead of PVDF membrane. Both WT and LH3 KO collagen $\alpha1\alpha1\alpha2$(IV) were measured in 0.2 M acetic acid at 10 °C. The denatured WT collagen $\alpha1\alpha1\alpha2$(IV) was measured using the cuvette after the measurements at 10 °C with heating up to 65 °C for 1 hour. The spectra represent the average of at least 3 scans recorded at a wavelength resolution of 0.1 nm.

Surface Plasmon Resonance (SPR) analysis – SPR experiments were carried out using a BIAcore X instrument (GE Healthcare, Chicago, IL, USA). Purified WT and LH3 KO collagen $\alpha1\alpha1\alpha2$(IV) were immobilized on a CM5 sensor chip by amide coupling. The approximate coupled protein concentration was 1.2 ng/mm^2 (1,200 response units) and 1.4 ng/mm^2 (1,400 response units) of WT and LH3 KO collagen $\alpha1\alpha1\alpha2$(IV), respectively. The experiments were performed at 20˚C in HBS-P (10 mM Hepes, pH 7.4, containing 150 mM NaCl and 0.005% Surfactant P20) using a flow rate of 10 µl/min. All curves are the average of at least three replicates and three independent measurements were performed. For the analysis of the binding affinity, the curves were fitted with the Langmuir binding model (BIAevaluation software; GE Healthcare). Hsp47 were purified from 17-day-old chicken embryos using methods described previously (77).

PTMs analysis by LC-MS – The hydroxylation rate of Lys (Lys + Hyl = 100%) and Pro (Pro + 4-Hyp + 3-Hyp = 100%) in each α chain of collagens $\alpha1\alpha1\alpha2$(IV), $\alpha1\alpha1\alpha2$(I) and $\alpha1\alpha1\alpha1$(III) was evaluated by LC-MS after acid hydrolysis, as described previously (78). In brief, after respective α chains were transferred to PVDF membranes as described in SDS-gel analysis above, the membrane bands were excised and subjected to acid hydrolysis (6 N HCl/1% phenol, 110°C for 20 h in the gas phase under N_2) after adding stable isotope-labeled collagen (SI-collagen) (79) as an internal standard. The acid hydrolysates were analyzed by LC-MS in multiple reaction monitoring (MRM) mode on a QTRAP 5500+ hybrid triple quadrupole/linear ion trap mass spectrometer (AB Sciex) coupled to an ExionLC AD HPLC system (AB Sciex) with a ZIC-HILIC column (3.5 µm particle size, L× I.D. 150 mm × 2.1 mm; Merck Millipore, Billerica, MA). The content of Pro, 3-Hyp, 4-Hyp, Lys and Hyl was quantitated by the peak area ratio of the analytes relative to the corresponding stable isotopically heavy analytes derived from SI-collagen (79). The occupancy of *O*-glycosylations attached to Hyl (free Hyl + galactosyl hydroxylysine + glucosyl galactosyl hydroxylysine = 100) in the collagens $\alpha1\alpha1\alpha2$(I) and $\alpha1\alpha1\alpha1$(III) mixture and purified collagen $\alpha1\alpha1\alpha2$(IV) was evaluated by LC-MS after alkaline hydrolysis, as described previously (79). In brief, the purified collagen samples were subjected to alkaline hydrolysis (2 N NaOH, 110°C for 20 h under N_2) after adding SI-collagen as the internal standard. The content of free Hyl, galactosyl hydroxylysine and glucosyl galactosyl hydroxylysine was quantitated by LC-MS analysis of the alkaline hydrolysates as described above.

Human material and ethics statement – 113 unrelated fetuses affected by an intracerebral hemorrhage (ICH) grade III or IV were included following termination of pregnancy (TOP) or intrauterine fetal death (IUFD). They were referred for *COL4A1/COL4A2* screening to the French national molecular genetics reference center for inherited cerebrovascular disorders (Saint Louis hospital, Paris) and shown to be negative using a targeted high throughput sequencing (conditions available upon request). Fetal ICH was in most cases detected at systematic 2nd and 3rd trimester ultrasound examinations and in some cases confirmed by fetal MRI and/or pathological examination. Systematic review of medical charts was performed in order to exclude fetuses with an identifiable cause or known risk factor for ICH, including evidence of maternal trauma during pregnancy, cocaine or maternal drug use, maternal or neonatal infections and fetal alloimmune thrombocytopenia. Written informed consent for genetic investigation and research was provided by parents in accordance with the declaration of Helsinki and the French law. This study has been approved by the Inserm Ethics Committee (INSERM IRB 00003888). Genomic DNA was isolated from post mortem fetal tissue and from peripheral blood leukocytes of both parents

and relatives when available. Prior to whole exome sequencing, we excluded the presence of a mutation in *COL4A1* and *COL4A2* genes by performing a targeted high throughput sequencing (conditions available upon request).

Exome sequencing – Exon capture was performed at the IntegraGen platform (Evry, France) for fetus probands and relatives using the SureSelect Human All Exon V5-UTR (Agilent technologies) or the Twist Human Core Exome Enrichment System (Twist Bioscience). Followed by 100 base pair paired-end sequencing using an Illumina NovaSeq platform. Data analysis was performed with the Integragen in house bioinformatic pipeline. Sequence reads were aligned to the human genome reference GRCh38/hg38 using BWA. Variant calling for the identification of SNVs (Single Nucleotide Variations) and small insertions/deletions was performed via the Broad Institute's GATK Haplotype Caller GVCF tool (GATK 3.8.1). Ensembl's VEP (Variant Effect Predictor, release VEP 95.1) program was used to process variants for further annotations. Allele frequency annotations was based on gnomAD (v2.1.1) and 1000Genomes datasets. PolyPhen-2 algorithm was used to predict deleteriousness of missense variants. Finally, we used CANOES for the detection of copy number variation (CNV) in whole exome sequencing data (Backenroth et al., 2014).

Qualifying variants in the PLOD3 gene – Several criteria were used for the selection of qualifying variants in the *PLOD3* gene: 1) Quality control: a minimum of 10 reads was required for depth coverage and a minimum of 25% for allelic balance, 2) Variants' nature: all coding and splice site variants were retained, 3) minor allele frequency (MAF) ≤ 1/1000 in external databases (gnomAD v2.1.1 and 1000Genomes Phase 3), and 4) for missense variants, predicted possibly or probably damaging with PolyPhen-2. Investigation for variant enrichment in the *PLOD3* gene was performed by comparing our fetus cohort (N=113) to cohorts of control individuals in gnomAD v2.1 and v3.1 with the same filter criteria. Burden tests / p-values were used for statistical analyses.

Mapping of the amino acid residues in protein structure – The human LH3 crystal structure was retrieved from the RCSB Protein Data Bank (www.rcsb.org, accession number 6FXK) and used for variant modelling using the UCSF Chimera software (version 1.14, build 42094).

Statistical analyses – For comparisons between two groups, one-way ANOVA was performed to determine whether differences between groups are significant using ORIGIN Pro ver. 9.1 (OriginLab Corp). A *p*-value of less than 0.05 was considered statistically significant.

Data availability – All data are contained within the article and supporting information. All source data are available from the corresponding author upon reasonable request. The MS data sets for protein identification of collagen $\alpha1\alpha1\alpha2$(IV) samples have been deposited to the ProteomeXchange consortium via the jPOST partner repository with the data set identifier PXD035051 (review only access site, https://repository.jpostdb.org/preview/89664503162be53c0b0771, with access key 8892).
(References: https://www.nature.com/articles/nbt.2839 and https://academic.oup.com/nar/article/45/D1/D1107/2605695?login=false).

Supporting information – This article contains supporting information.

Acknowledgments — We gratefully acknowledge the research department of Shriners Hospitals for Children in Portland for using CD instrument. We thank Hans Peter Bächinger and Cassandre Labelle-Dumais for useful discussions and suggestions on this work.

Author contributions—YI, ETL, and DBG. were responsible for the overall design of the study. YI, YT, TC, SFT, and DRK conducted and analyzed the experiments. YI, YT, TC, SFT, DRK, KM, ETL, and DBG provided essential material, reviewed, and discussed the results. YI and DBG wrote the main article text and all authors were involved in editing the article.

Funding and additional information
Research reported in this publication was supported by All May See Foundation award 7031182 (YI), the National Institutes of Health (NIH) under Award Number R01NS096173 (DBG), and in part by the UCSF Vision Core shared resource of the NIH/NEI P30 EY002162, and by an unrestricted grant from Research to Prevent Blindness, New York, NY. The content of this publication is solely the responsibility of the authors and does not necessarily represent the official views of the National Institutes of Health or other funding agencies.

Conflict of interest—The authors declare that they have no competing interests related to this work.

Abbreviations—The abbreviations used are: ER; endoplasmic reticulum, PTM; post-translational modification, 4Hyp; 4-hydroxyproline, 3Hyp; 3-hydroxyproline, Hyl; hydroxylysine, LH; lysyl hydroxylase, EDS; Ehlers-Danlos syndrome, OI; Osteogenesis Imperfecta, MEFs; mouse embryonic fibroblasts, KO; knockout, WT; wild-type, AHA; L-azidohomoalanine, CD; circular dichroism, AAA; amino acid analyses, P4H; prolyl 4-hydroxylases.

References

1. Bella, J., and Hulmes, D. J. (2017) Fibrillar Collagens. *Subcell Biochem* **82**, 457-490
2. Ricard-Blum, S., and Ruggiero, F. (2005) The collagen superfamily: from the extracellular matrix to the cell membrane. *Pathologie Biologie* **53**, 430-442
3. Lamande, S. R., and Bateman, J. F. (2020) Genetic Disorders of the Extracellular Matrix. *Anat Rec (Hoboken)* **303**, 1527-1542
4. Bateman, J. F., Boot-Handford, R. P., and Lamande, S. R. (2009) Genetic diseases of connective tissues: cellular and extracellular effects of ECM mutations. *Nat Rev Genet* **10**, 173-183
5. Marini, J. C., Forlino, A., Bachinger, H. P., Bishop, N. J., Byers, P. H., Paepe, A., Fassier, F., Fratzl-Zelman, N., Kozloff, K. M., Krakow, D., Montpetit, K., and Semler, O. (2017) Osteogenesis imperfecta. *Nat Rev Dis Primers* **3**, 17052
6. Malfait, F., Castori, M., Francomano, C. A., Giunta, C., Kosho, T., and Byers, P. H. (2020) The Ehlers-Danlos syndromes. *Nat Rev Dis Primers* **6**, 64
7. Besio, R., Chow, C. W., Tonelli, F., Marini, J. C., and Forlino, A. (2019) Bone biology: insights from osteogenesis imperfecta and related rare fragility syndromes. *FEBS J* **286**, 3033-3056
8. Claeys, L., Storoni, S., Eekhoff, M., Elting, M., Wisse, L., Pals, G., Bravenboer, N., Maugeri, A., and Micha, D. (2021) Collagen transport and related pathways in Osteogenesis Imperfecta. *Hum Genet* **140**, 1121-1141
9. Omar, R., Malfait, F., and Van Agtmael, T. (2021) Four decades in the making: Collagen III and mechanisms of vascular Ehlers Danlos Syndrome. *Matrix Biol Plus* **12**, 100090
10. Van Damme, T., Colman, M., Syx, D., and Malfait, F. (2022) The Ehlers-Danlos Syndromes against the Backdrop of Inborn Errors of Metabolism. *Genes (Basel)* **13**
11. Hudson, B. G., Tryggvason, K., Sundaramoorthy, M., and Neilson, E. G. (2003) Alport's syndrome, Goodpasture's syndrome, and type IV collagen. *N Engl J Med* **348**, 2543-2556
12. Boudko, S. P., Pokidysheva, E., and Hudson, B. G. (2022) Prospective collagen IValpha345 therapies for Alport syndrome. *Curr Opin Nephrol Hypertens* **31**, 213-220
13. Jeanne, M., and Gould, D. B. (2017) Genotype-phenotype correlations in pathology caused by collagen type IV alpha 1 and 2 mutations. *Matrix Biol* **57-58**, 29-44
14. Mao, M., Alavi, M. V., Labelle-Dumais, C., and Gould, D. B. (2015) Type IV Collagens and Basement Membrane Diseases: Cell Biology and Pathogenic Mechanisms. *Curr Top Membr* **76**, 61-116
15. Kuo, D. S., Labelle-Dumais, C., and Gould, D. B. (2012) COL4A1 and COL4A2 mutations and disease: insights into pathogenic mechanisms and potential therapeutic targets. *Hum Mol Genet* **21**, R97-110
16. Boyce, D., McGee, S., Shank, L., Pathak, S., and Gould, D. (2021) Epilepsy and related challenges in children with COL4A1 and COL4A2 mutations: A Gould syndrome patient registry. *Epilepsy Behav* **125**, 108365
17. Mao, M., Kiss, M., Ou, Y., and Gould, D. B. (2017) Genetic dissection of anterior segment dysgenesis caused by a Col4a1 mutation in mouse. *Dis Model Mech* **10**, 475-485

18. Mao, M., Smith, R. S., Alavi, M. V., Marchant, J. K., Cosma, M., Libby, R. T., John, S. W., and Gould, D. B. (2015) Strain-Dependent Anterior Segment Dysgenesis and Progression to Glaucoma in Col4a1 Mutant Mice. *Invest Ophthalmol Vis Sci* **56**, 6823-6831
19. Ishikawa, Y., and Bachinger, H. P. (2013) A molecular ensemble in the rER for procollagen maturation. *Biochim Biophys Acta* **1833**, 2479-2491
20. Ito, S., and Nagata, K. (2021) Quality Control of Procollagen in Cells. *Annu Rev Biochem* **90**, 631-658
21. Onursal, C., Dick, E., Angelidis, I., Schiller, H. B., and Staab-Weijnitz, C. A. (2021) Collagen Biosynthesis, Processing, and Maturation in Lung Ageing. *Front Med (Lausanne)* **8**, 593874
22. Ihme, A., Krieg, T., Nerlich, A., Feldmann, U., Rauterberg, J., Glanville, R. W., Edel, G., and Muller, P. K. (1984) Ehlers-Danlos syndrome type VI: collagen type specificity of defective lysyl hydroxylation in various tissues. *J Invest Dermatol* **83**, 161-165
23. Weis, M. A., Hudson, D. M., Kim, L., Scott, M., Wu, J. J., and Eyre, D. R. (2010) Location of 3-hydroxyproline residues in collagen types I, II, III, and V/XI implies a role in fibril supramolecular assembly. *J Biol Chem* **285**, 2580-2590
24. Ishikawa, Y., Taga, Y., Zientek, K., Mizuno, N., Salo, A. M., Semenova, O., Tufa, S. F., Keene, D. R., Holden, P., Mizuno, K., Gould, D. B., Myllyharju, J., and Bachinger, H. P. (2021) Type I and type V procollagen triple helix uses different subsets of the molecular ensemble for lysine posttranslational modifications in the rER. *J Biol Chem* **296**, 100453
25. Ishikawa, Y., and Bächinger, H. P. (2014) A Substrate Preference for the Rough Endoplasmic Reticulum Resident Protein FKBP22 during Collagen Biosynthesis. *Journal of Biological Chemistry* **289**, 18189-18201
26. Taga, Y., Kusubata, M., Ogawa-Goto, K., and Hattori, S. (2016) Developmental Stage-dependent Regulation of Prolyl 3-Hydroxylation in Tendon Type I Collagen. *J Biol Chem* **291**, 837-847
27. Salo, A. M., and Myllyharju, J. (2021) Prolyl and lysyl hydroxylases in collagen synthesis. *Exp Dermatol* **30**, 38-49
28. Basak, T., Vega-Montoto, L., Zimmerman, L. J., Tabb, D. L., Hudson, B. G., and Vanacore, R. M. (2016) Comprehensive Characterization of Glycosylation and Hydroxylation of Basement Membrane Collagen IV by High-Resolution Mass Spectrometry. *J Proteome Res* **15**, 245-258
29. Berg, R. A., and Prockop, D. J. (1973) The thermal transition of a non-hydroxylated form of collagen. Evidence for a role for hydroxyproline in stabilizing the triple-helix of collagen. *Biochem Biophys Res Commun* **52**, 115-120
30. Mizuno, K., Hayashi, T., Peyton, D. H., and Bachinger, H. P. (2004) Hydroxylation-induced stabilization of the collagen triple helix. Acetyl-(glycyl-4(R)-hydroxyprolyl-4(R)-hydroxyprolyl)(10)-NH(2) forms a highly stable triple helix. *J Biol Chem* **279**, 38072-38078
31. Taga, Y., Tanaka, K., Hattori, S., and Mizuno, K. (2021) In-depth correlation analysis demonstrates that 4-hydroxyproline at the Yaa position of Gly-Xaa-Yaa repeats dominantly stabilizes collagen triple helix. *Matrix Biol Plus* **10**, 100067
32. Montgomery, N. T., Zientek, K. D., Pokidysheva, E. N., and Bachinger, H. P. (2018) Post-translational modification of type IV collagen with 3-hydroxyproline affects its interactions with glycoprotein VI and nidogens 1 and 2. *J Biol Chem* **293**, 5987-5999
33. Grafe, I., Yang, T., Alexander, S., Homan, E. P., Lietman, C., Jiang, M. M., Bertin, T., Munivez, E., Chen, Y., Dawson, B., Ishikawa, Y., Weis, M. A., Sampath, T. K., Ambrose, C., Eyre, D., Bachinger, H. P., and Lee, B. (2014) Excessive transforming growth factor-beta signaling is a common mechanism in osteogenesis imperfecta. *Nat Med* **20**, 670-675
34. Hennet, T. (2019) Collagen glycosylation. *Curr Opin Struct Biol* **56**, 131-138
35. De Giorgi, F., Fumagalli, M., Scietti, L., and Forneris, F. (2021) Collagen hydroxylysine glycosylation: non-conventional substrates for atypical glycosyltransferase enzymes. *Biochem Soc Trans* **49**, 855-866
36. Geister, K. A., Lopez-Jimenez, A. J., Houghtaling, S., Ho, T. H., Vanacore, R., and Beier, D. R. (2019) Loss of function of Colgalt1 disrupts collagen post-translational modification and causes musculoskeletal defects. *Dis Model Mech* **12**
37. Miyatake, S., Schneeberger, S., Koyama, N., Yokochi, K., Ohmura, K., Shiina, M., Mori, H., Koshimizu, E., Imagawa, E., Uchiyama, Y., Mitsuhashi, S., Frith, M. C., Fujita, A., Satoh, M., Taguri, M., Tomono, Y., Takahashi, K., Doi, H., Takeuchi, H., Nakashima, M., Mizuguchi, T., Takata, A., Miyake, N., Saitsu, H., Tanaka, F., Ogata, K., Hennet, T., and Matsumoto, N. (2018) Biallelic COLGALT1 variants are associated with cerebral small vessel disease. *Ann Neurol* **84**, 843-853

38. Teunissen, M. W. A., Kamsteeg, E. J., Sallevelt, S., Pennings, M., Bauer, N. J. C., Vermeulen, R. J., and Nicolai, J. (2021) Biallelic Variants in the COLGALT1 Gene Causes Severe Congenital Porencephaly: A Case Report. *Neurol Genet* **7**, e564
39. Salo, A. M., Cox, H., Farndon, P., Moss, C., Grindulis, H., Risteli, M., Robins, S. P., and Myllyla, R. (2008) A connective tissue disorder caused by mutations of the lysyl hydroxylase 3 gene. *Am J Hum Genet* **83**, 495-503
40. Ewans, L. J., Colley, A., Gaston-Massuet, C., Gualtieri, A., Cowley, M. J., McCabe, M. J., Anand, D., Lachke, S. A., Scietti, L., Forneris, F., Zhu, Y., Ying, K., Walsh, C., Kirk, E. P., Miller, D., Giunta, C., Sillence, D., Dinger, M., Buckley, M., and Roscioli, T. (2019) Pathogenic variants in PLOD3 result in a Stickler syndrome-like connective tissue disorder with vascular complications. *J Med Genet* **56**, 629-638
41. Vahidnezhad, H., Youssefian, L., Saeidian, A. H., Touati, A., Pajouhanfar, S., Baghdadi, T., Shadmehri, A. A., Giunta, C., Kraenzlin, M., Syx, D., Malfait, F., Has, C., Lwin, S. M., Karamzadeh, R., Liu, L., Guy, A., Hamid, M., Kariminejad, A., Zeinali, S., McGrath, J. A., and Uitto, J. (2019) Mutations in PLOD3, encoding lysyl hydroxylase 3, cause a complex connective tissue disorder including recessive dystrophic epidermolysis bullosa-like blistering phenotype with abnormal anchoring fibrils and type VII collagen deficiency. *Matrix Biol* **81**, 91-106
42. Maddirevula, S., Alzahrani, F., Al-Owain, M., Al Muhaizea, M. A., Kayyali, H. R., AlHashem, A., Rahbeeni, Z., Al-Otaibi, M., Alzaidan, H. I., Balobaid, A., El Khashab, H. Y., Bubshait, D. K., Faden, M., Yamani, S. A., Dabbagh, O., Al-Mureikhi, M., Jasser, A. A., Alsaif, H. S., Alluhaydan, I., Seidahmed, M. Z., Alabbasi, B. H., Almogarri, I., Kurdi, W., Akleh, H., Qari, A., Al Tala, S. M., Alhomaidi, S., Kentab, A. Y., Salih, M. A., Chedrawi, A., Alameer, S., Tabarki, B., Shamseldin, H. E., Patel, N., Ibrahim, N., Abdulwahab, F., Samira, M., Goljan, E., Abouelhoda, M., Meyer, B. F., Hashem, M., Shaheen, R., AlShahwan, S., Alfadhel, M., Ben-Omran, T., Al-Qattan, M. M., Monies, D., and Alkuraya, F. S. (2019) Autozygome and high throughput confirmation of disease genes candidacy. *Genet Med* **21**, 736-742
43. Zhou, J., Feng, W., Zhuo, X., Lu, W., Wang, J., Fang, F., and Wang, X. Cerebral small vessel disease caused by PLOD3 mutation: Expanding the phenotypic spectrum of lysyl hydroxylase-3 deficiency. *Pediatric Investigation* **n/a**
44. Heikkinen, J., Risteli, M., Wang, C., Latvala, J., Rossi, M., Valtavaara, M., and Myllyla, R. (2000) Lysyl hydroxylase 3 is a multifunctional protein possessing collagen glucosyltransferase activity. *J Biol Chem* **275**, 36158-36163
45. Rautavuoma, K., Takaluoma, K., Passoja, K., Pirskanen, A., Kvist, A. P., Kivirikko, K. I., and Myllyharju, J. (2002) Characterization of three fragments that constitute the monomers of the human lysyl hydroxylase isoenzymes 1-3. The 30-kDa N-terminal fragment is not required for lysyl hydroxylase activity. *J Biol Chem* **277**, 23084-23091
46. Wang, C., Luosujarvi, H., Heikkinen, J., Risteli, M., Uitto, L., and Myllyla, R. (2002) The third activity for lysyl hydroxylase 3: galactosylation of hydroxylysyl residues in collagens in vitro. *Matrix Biol* **21**, 559-566
47. Ruotsalainen, H., Sipila, L., Vapola, M., Sormunen, R., Salo, A. M., Uitto, L., Mercer, D. K., Robins, S. P., Risteli, M., Aszodi, A., Fassler, R., and Myllyla, R. (2006) Glycosylation catalyzed by lysyl hydroxylase 3 is essential for basement membranes. *J Cell Sci* **119**, 625-635
48. Scietti, L., Chiapparino, A., De Giorgi, F., Fumagalli, M., Khoriauli, L., Nergadze, S., Basu, S., Olieric, V., Cucca, L., Banushi, B., Profumo, A., Giulotto, E., Gissen, P., and Forneris, F. (2018) Molecular architecture of the multifunctional collagen lysyl hydroxylase and glycosyltransferase LH3. *Nat Commun* **9**, 3163
49. Guo, H. F., Bota-Rabassedas, N., Terajima, M., Leticia Rodriguez, B., Gibbons, D. L., Chen, Y., Banerjee, P., Tsai, C. L., Tan, X., Liu, X., Yu, J., Tokmina-Roszyk, M., Stawikowska, R., Fields, G. B., Miller, M. D., Wang, X., Lee, J., Dalby, K. N., Creighton, C. J., Phillips, G. N., Jr., Tainer, J. A., Yamauchi, M., and Kurie, J. M. (2021) A collagen glucosyltransferase drives lung adenocarcinoma progression in mice. *Commun Biol* **4**, 482
50. Rautavuoma, K., Takaluoma, K., Sormunen, R., Myllyharju, J., Kivirikko, K. I., and Soininen, R. (2004) Premature aggregation of type IV collagen and early lethality in lysyl hydroxylase 3 null mice. *Proc Natl Acad Sci U S A* **101**, 14120-14125
51. Sipila, L., Ruotsalainen, H., Sormunen, R., Baker, N. L., Lamande, S. R., Vapola, M., Wang, C., Sado, Y., Aszodi, A., and Myllyla, R. (2007) Secretion and assembly of type IV and VI collagens depend on glycosylation of hydroxylysines. *J Biol Chem* **282**, 33381-33388

52. Duncan, K. G., Fessler, L. I., Bachinger, H. P., and Fessler, J. H. (1983) Procollagen IV. Association to tetramers. *J Biol Chem* **258**, 5869-5877
53. Mirigian, L. S., Makareeva, E., and Leikin, S. (2014) Pulse-chase analysis of procollagen biosynthesis by azidohomoalanine labeling. *Connect Tissue Res* **55**, 403-410
54. Syx, D., Ishikawa, Y., Gebauer, J., Boudko, S. P., Guillemyn, B., Van Damme, T., D'Hondt, S., Symoens, S., Nampoothiri, S., Gould, D. B., Baumann, U., Bachinger, H. P., and Malfait, F. (2021) Aberrant binding of mutant HSP47 affects posttranslational modification of type I collagen and leads to osteogenesis imperfecta. *PLoS Genet* **17**, e1009339
55. Fessler, L. I., and Fessler, J. H. (1982) Identification of the carboxyl peptides of mouse procollagen IV and its implications for the assembly and structure of basement membrane procollagen. *J Biol Chem* **257**, 9804-9810
56. Lunstrum, G. P., Bachinger, H. P., Fessler, L. I., Duncan, K. G., Nelson, R. E., and Fessler, J. H. (1988) Drosophila basement membrane procollagen IV. I. Protein characterization and distribution. *J Biol Chem* **263**, 18318-18327
57. Toth, M., Sado, Y., Ninomiya, Y., and Fridman, R. (1999) Biosynthesis of alpha2(IV) and alpha1(IV) chains of collagen IV and interactions with matrix metalloproteinase-9. *J Cell Physiol* **180**, 131-139
58. Matsuoka, Y., Kubota, H., Adachi, E., Nagai, N., Marutani, T., Hosokawa, N., and Nagata, K. (2004) Insufficient folding of type IV collagen and formation of abnormal basement membrane-like structure in embryoid bodies derived from Hsp47-null embryonic stem cells. *Mol Biol Cell* **15**, 4467-4475
59. Ishida, Y., Kubota, H., Yamamoto, A., Kitamura, A., Bachinger, H. P., and Nagata, K. (2006) Type I collagen in Hsp47-null cells is aggregated in endoplasmic reticulum and deficient in N-propeptide processing and fibrillogenesis. *Mol Biol Cell* **17**, 2346-2355
60. Vranka, J. A., Pokidysheva, E., Hayashi, L., Zientek, K., Mizuno, K., Ishikawa, Y., Maddox, K., Tufa, S., Keene, D. R., Klein, R., and Bachinger, H. P. (2010) Prolyl 3-hydroxylase 1 null mice display abnormalities in fibrillar collagen-rich tissues such as tendons, skin, and bones. *J Biol Chem* **285**, 17253-17262
61. Pedchenko, V., Bauer, R., Pokidysheva, E. N., Al-Shaer, A., Forde, N. R., Fidler, A. L., Hudson, B. G., and Boudko, S. P. (2019) A chloride ring is an ancient evolutionary innovation mediating the assembly of the collagen IV scaffold of basement membranes. *J Biol Chem* **294**, 7968-7981
62. Ivanov, S. V., Bauer, R., Pokidysheva, E. N., and Boudko, S. P. (2021) Collagen IV Exploits a Cl- Step Gradient for Scaffold Assembly. *Adv Exp Med Biol* **21**, 129-141
63. Bhatnagar, R. S., and Gough, C. A. (1996) Circular Dichroism of Collagen and Related Polypeptides. in *Circular Dichroism and the Conformational Analysis of Biomolecules* (Fasman, G. D. ed.), Springer US, Boston, MA. pp 183-199
64. Ono, T., Miyazaki, T., Ishida, Y., Uehata, M., and Nagata, K. (2012) Direct in vitro and in vivo evidence for interaction between Hsp47 protein and collagen triple helix. *J Biol Chem* **287**, 6810-6818
65. Ishikawa, Y., Ito, S., Nagata, K., Sakai, L. Y., and Bachinger, H. P. (2016) Intracellular mechanisms of molecular recognition and sorting for transport of large extracellular matrix molecules. *Proc Natl Acad Sci U S A* **113**, E6036-E6044
66. Sricholpech, M., Perdivara, I., Yokoyama, M., Nagaoka, H., Terajima, M., Tomer, K. B., and Yamauchi, M. (2012) Lysyl hydroxylase 3-mediated glucosylation in type I collagen: molecular loci and biological significance. *J Biol Chem* **287**, 22998-23009
67. Gould, D. B., Phalan, F. C., Breedveld, G. J., van Mil, S. E., Smith, R. S., Schimenti, J. C., Aguglia, U., van der Knaap, M. S., Heutink, P., and John, S. W. (2005) Mutations in Col4a1 cause perinatal cerebral hemorrhage and porencephaly. *Science* **308**, 1167-1171
68. Gould, D. B., Phalan, F. C., van Mil, S. E., Sundberg, J. P., Vahedi, K., Massin, P., Bousser, M. G., Heutink, P., Miner, J. H., Tournier-Lasserve, E., and John, S. W. (2006) Role of COL4A1 in small-vessel disease and hemorrhagic stroke. *N Engl J Med* **354**, 1489-1496
69. Breedveld, G., de Coo, I. F., Lequin, M. H., Arts, W. F., Heutink, P., Gould, D. B., John, S. W., Oostra, B., and Mancini, G. M. (2006) Novel mutations in three families confirm a major role of COL4A1 in hereditary porencephaly. *J Med Genet* **43**, 490-495
70. Vahedi, K., Boukobza, M., Massin, P., Gould, D. B., Tournier-Lasserve, E., and Bousser, M. G. (2007) Clinical and brain MRI follow-up study of a family with COL4A1 mutation. *Neurology* **69**, 1564-1568
71. Coste, T., Vincent-Delorme, C., Stichelbout, M., Devisme, L., Gelot, A., Deryabin, I., Pelluard, F., Aloui, C., Leutenegger, A. L., Jouannic, J. M., Heron, D., Gould, D. B., and Tournier-Lasserve, E. (2022)

COL4A1/COL4A2 and inherited platelet disorder gene variants in fetuses showing intracranial hemorrhage. *Prenat Diagn* **42**, 601-610

72. Aro, E., Salo, A. M., Khatri, R., Finnila, M., Miinalainen, I., Sormunen, R., Pakkanen, O., Holster, T., Soininen, R., Prein, C., Clausen-Schaumann, H., Aszodi, A., Tuukkanen, J., Kivirikko, K. I., Schipani, E., and Myllyharju, J. (2015) Severe Extracellular Matrix Abnormalities and Chondrodysplasia in Mice Lacking Collagen Prolyl 4-Hydroxylase Isoenzyme II in Combination with a Reduced Amount of Isoenzyme I. *J Biol Chem* **290**, 16964-16978
73. Zou, Y., Donkervoort, S., Salo, A. M., Foley, A. R., Barnes, A. M., Hu, Y., Makareeva, E., Leach, M. E., Mohassel, P., Dastgir, J., Deardorff, M. A., Cohn, R. D., DiNonno, W. O., Malfait, F., Lek, M., Leikin, S., Marini, J. C., Myllyharju, J., and Bonnemann, C. G. (2017) P4HA1 mutations cause a unique congenital disorder of connective tissue involving tendon, bone, muscle and the eye. *Hum Mol Genet* **26**, 2207-2217
74. Al-Shaer, A., Lyons, A., Ishikawa, Y., Hudson, B. G., Boudko, S. P., and Forde, N. R. (2021) Sequence-dependent mechanics of collagen reflect its structural and functional organization. *Biophys J* **120**, 4013-4028
75. Taga, Y., Kusubata, M., Ogawa-Goto, K., and Hattori, S. (2012) Development of a novel method for analyzing collagen O-glycosylations by hydrazide chemistry. *Mol Cell Proteomics* **11**, M111 010397
76. Morris, N. P., Keene, D. R., Glanville, R. W., Bentz, H., and Burgeson, R. E. (1986) The tissue form of type VII collagen is an antiparallel dimer. *J Biol Chem* **261**, 5638-5644
77. Macdonald, J. R., and Bachinger, H. P. (2001) HSP47 binds cooperatively to triple helical type I collagen but has little effect on the thermal stability or rate of refolding. *J Biol Chem* **276**, 25399-25403
78. Fujii, K. K., Taga, Y., Sakai, T., Ito, S., Hattori, S., Nagata, K., and Koide, T. (2019) Lowering the culture temperature corrects collagen abnormalities caused by HSP47 gene knockout. *Sci Rep* **9**, 17433
79. Taga, Y., Kusubata, M., Ogawa-Goto, K., and Hattori, S. (2014) Stable isotope-labeled collagen: a novel and versatile tool for quantitative collagen analyses using mass spectrometry. *J Proteome Res* **13**, 3671-3678

Figure legends

Figure 1. LH3 deficiency in PFHR9 cells impairs collagen α1α1α2(IV) secretion.
(A) Semi-quantitative Western blots showing successful ablation of LH3 in PFHR9 cells following CRISPR/Cas9 mediated LH3 inactivation (LH3 KO PFHR9 cells). β-tubulin was used as a loading control. **(B)** Semi-quantitative Western blots and quantification of COL4A1 and COL4A2 levels in the conditioned cell culture medium showing reduced secretion of COL4A1 and COL4A2 in LH3 KO PFHR9 cells (KO) compared to their wild-type (WT) controls. Laminin α/β/γ was used as a loading control. **(C)** Semi-quantitative Western blots and quantification of COL4A1 and COL4A2 levels in cell lysates showing intracellular COL4A1 accumulation in LH3 KO PFHR9 cells. β-tubulin was used as a loading control. COL4 indicates control purified collagen α1α1α2(IV). The quantification data in B and C are shown as fold relative to WT levels and presented as means ± SD with individual data points representing independent preparations of culture medium and cell lysate and (n = 3). **(D)** Representative SDS-PAGE gel (top) and quantification (bottom) of time dependent extracellular collagen α1α1α2(IV) levels in WT PFHR9 cells measured by AHA-Alexa Fluor pulse-chase labeling. 'ctrl' indicates purified AHA incorporated collagen α1α1α2(IV). The quantification of AHA incorporated collagen α1α1α2(IV) was set to 1.0 at 480 minutes (n = 5). **(E)** Representative SDS-PAGE gel (top) and quantification (bottom) of time dependent extracellular collagen α1α1α2(IV) levels for LH3 KO PFHR9 cells measured by AHA-Alexa Fluor pulse-chase labeling, demonstrating significantly impaired collagen α1α1α2(IV) secretion in LH3 KO PFHR9 cells compared to their WT AHA incorporated collagen α1α1α2(IV) controls at 8 hours (n = 5). Source data files for Figure 1: The uncropped images of Western blots used in Figure 1A-C are presented in Figure S2, generation of the purified AHA incorporated collagen α1α1α2(IV) used as a control in Figure 1D is presented Figure S3, the value of AHA incorporated collagen α1α1α2(IV) at each time points are shown in Supporting Table 1.

Figure 2. LH3 deficiency in MEFs does not impair biosynthesis of collagen α1α1α2(I) or collagen α1α1α1(III).
(A) Semi-quantitative Western blots showing successful ablation of LH3 in MEFs following CRISPR/Cas9 mediated LH3 inactivation (LH3 KO MEFs). β-actin was used as a loading control. **(B)** Semi-quantitative Western blots and quantification of collagen α1α1α2(I) in conditioned cell culture medium showing increased secretion of ProCOL1A1 and ProCOL1A2 in LH3 KO MEFs (KO) compared to their wild-type (WT) controls. Fibronectin was used as a loading control. COL1 indicates purified pepsin treated collagen α1α1α2(I). The quantification data in B are shown as fold relative to WT levels and presented as means ± SD with individual data points representing independent preparations of culture medium (n = 3). **(C)** Representative SDS-PAGE gel and **(D)** quantification of time dependent extracellular levels of collagens α1α1α2(I) and α1α1α1(III) measured by AHA-Alexa Fluor pulse-chase labeling, demonstrating comparable secretion rate between LH3 KO and WT MEFs. 'ctrl' indicates purified AHA incorporated collagens α1α1α2 (I) and α1α1α1(III). WT AHA incorporation signal was set to 1.0 at 180 minutes (n=5). Source data files for Figure 2: The uncropped images of Western blots used in Figure 2A and 2B are presented in Figure S5, generation of the purified AHA incorporated pepsin treated collagens α1α1α2(I) and α1α1α1(III) mixture used as a control in Figure 2C is presented Figure S6, the value of AHA incorporated collagens α1α1α2(I) and α1α1α1(III) at each time points are shown in Supporting Table 2.

Figure 3. LH3 deficiency impairs collagen α1α1α2(IV) oligomerization and triple helix formation.
(A) Representative Coomassie blue stained 3-8 % Tris/Acetate gel showing pepsin-treated collagens α1α1α2(I) and α1α1α1(III) purified from conditioned culture medium of WT and LH3 KO MEFs. **(B)** Representative Coomassie blue stained 3.5 % SDS-Agarose gel showing collagen α1α1α2(IV) purified from conditioned culture medium of WT and LH3 KO PFHR9 cells. **(C)** Representative transmission electron rotary shadow microscopy images showing structural alterations collagen α1α1α2(IV) purified from conditioned culture medium of WT and LH3 KO PFHR9 cells. Arrowheads point to globular NC1 domains. Diagram at the bottom left illustrates normal collagen α1α1α2(IV) network formation. The frequency of each molecular species is indicated in parentheses (%). **(D)** CD spectra of purified collagen α1α1α2(IV) from conditioned culture medium of WT and LH3 KO PFHR9 cells under native (10 ^{o}C) and denaturing (65 ^{o}C) conditions. **(E)** Surface plasmon resonance analysis showing concentration-dependent binding kinetics between HSP47 and collagen α1α1α2(IV) purified from conditioned culture medium of WT and LH3 KO PFHR9 cells. Each curve represents the average of a minimum of three measurements. The binding constants and affinities are shown as mean ± SD in the inset.

Figure 4. LH3 is a selective lysyl hydroxylase and general collagen glycosyltransferase.
(A) Acid hydrolysis amino acid analysis. Histograms showing the occupancy of post-translational modifications in proline (3Hyp + 4Hyp + Pro = 100 %) and lysine (Hyl + Lys = 100 %) in individual alpha chains of collagens α1α1α2(IV), α1α1α2(I) and α1α1α1(III). [3Hyp; 3-hydroxyproline, 4Hyp; 4-hydroxyproline, Pro; proline, Hyl; hydroxylysine. Lys; lysine]. **(B)** Alkaline hydrolysis amino acid analysis. Histogram showing the occupancy of *O*-glycosylation attached to hydroxylysine (GGHL + GHL + Hyl = 100) in purified collagens α1α1α2(IV) and mixture of collagens α1α1α2(I) and α1α1α1(III). [GGHL; glucosyl galactosyl hydroxylysine, GHL; galactosyl hydroxylysine, Hyl; hydroxylysine]. Source data files for Figure 4: The value of each amino acid, the number of biological replicates and detailed statistical analyses for data shown in Figure 4A and 4B are presented in Table S3 and Figure S8, respectively.

Figure 5. Identification of four rare *PLOD3* variants in fetal ICH cases.
(A) Genealogical trees of the three families with *PLOD3* variants. Square = male, circle = female, triangle = pregnancy not carried to term, black filled symbol = affected individual, empty symbol = clinically healthy relative, diagonal black line = deceased fetuses, syringe symbol = blood sampled individual. The age of termination of pregnancy is indicated under each case. (B) The crystal structure of the LH3 shows three different domains: catalytic glycosyltransferase domain (white), accessory glycosyltransferase domain (gray) and lysine dioxygenase domain (light blue). Missense variants identified in humans are indicated in different colors on the LH3 crystal structure. Green indicates previously reported variants have connective disorders resembling Stickler syndrome-like and Epidermolysis Bullosa. Magenta indicates variants identified in this study.

Table 1. Enrichment analysis of rare predicted damaging *PLOD3* variants in fetus cohort vs gnomAD cohorts.

	Number of loss of function and missense variants with a MAF ≤ 1/1000 in *PLOD3* gene	**P-value**
gnomAD v2.1 (N=141,456 individuals)	2160	0.69
gnomAD v3.1 (N=76,156 individuals)	1225	0.7

MAF: minor allele frequency

Table 2. Rare variants identified in *PLOD3* gene in the cohort of 113 ICH fetuses.

Fetus	HGVSc position (NM_001084.5)	Protein change	Variant class	Status	gnomAD v.2.1 AF	PolyPhen-2 prediction	ACMG Class
F09	c.593T>C	p.(L198P)	Missense	HTZ	0.0004%	Probably damaging (0.994)	3
F12*	c.589C>T	p.(R197W)	Missense	HTZ	0.0012%	Possibly damaging (0.735)	3
F12*	c.1466C>T	p.(P489L)	Missense	HTZ	0.051%	Possibly damaging (0.769)	3

HTZ: heterozygous, AF: allele frequency, *: biallelic variants (inherited from each parent). ClinVar accession numbers: SCV002558784 (p.L198P), SCV002558785 (p.R197W) and SCV002558786 (p.P489L).

Table 3: Main clinical and pathological features of ICH affected fetuses with *PLOD3* variants.

Fetus	**F09**	**F12**
Sex	Female	Female
Gestation at diagnosis (weeks)	31	30
Brian imaging findings	Microcephaly, Ventriculomegaly, Interhemispheric cyst, Porencephalic cavities, Thin corpus callosum	Asymmetric bilateral ventriculomegaly, Ischemic-hemorrhagic lesions in the right hemisphere
Outcome	TOP	TOP
Fetal brain examination	Important ventriculomegaly, White matter atrophy, Severe microcephaly with diffuse bilateral lesions, Absent or very thin corpus callosum	Asymmetric bilateral ventriculomegaly, Intraparenchymal hemorrhages with cortical and subcortical ischemic foci
Skeletal X-ray examination	No sign of bone abnormality except for the absence of the 12th right rib	No sign of bone abnormality
Other autopsy anomalies	No sign of external or visceral malformation	No sign of external or visceral malformation

TOP: termination of pregnancy

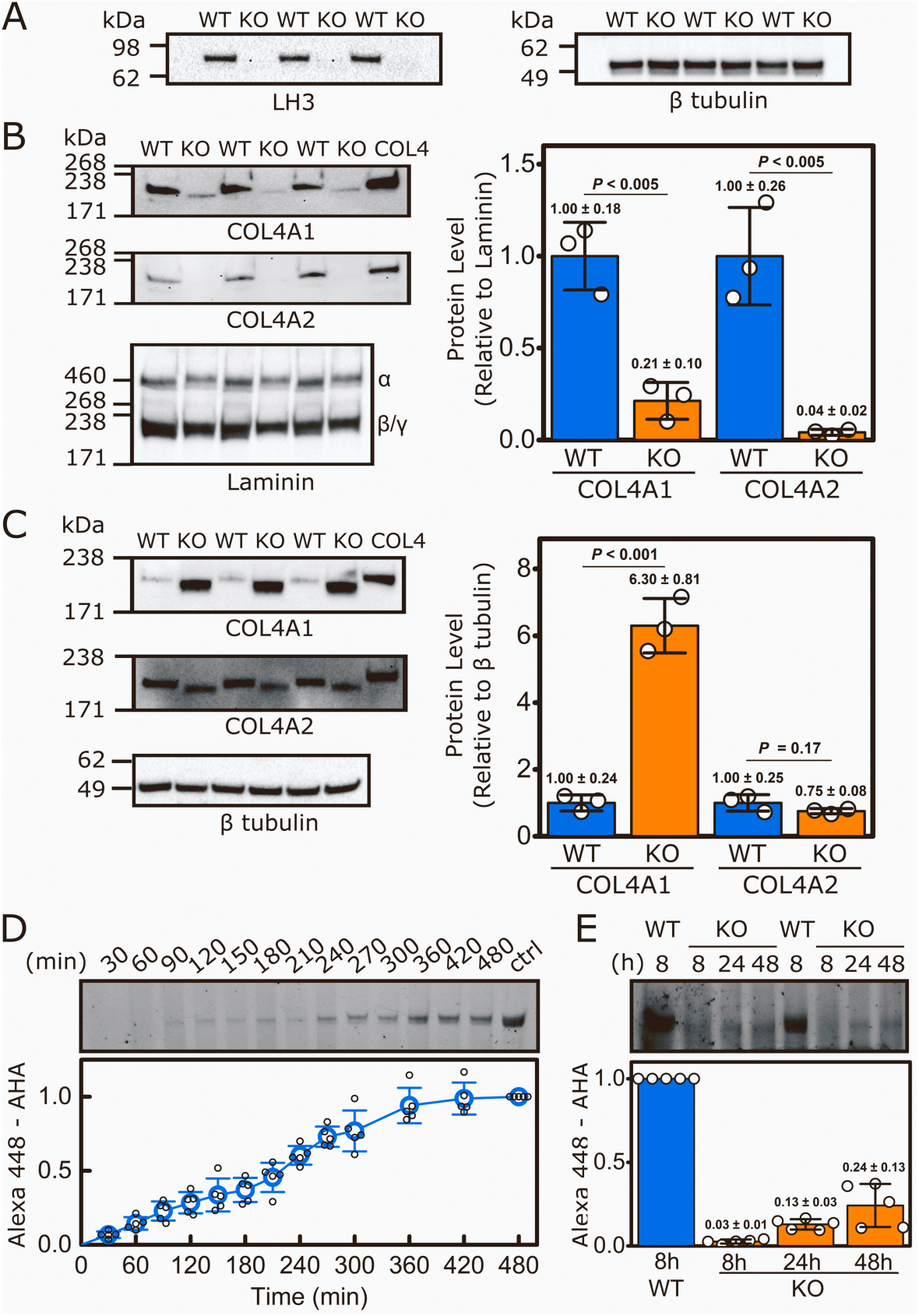
A
kDa
WT KO WT KO WT KO
98
62
LH3
kDa
WT KO WT KO WT KO
62
49
β tubulin
B
kDa
WT KO WT KO WT KO COL4
268
238
171
COL4A1
268
238
171
COL4A2
460
268
238
171
α
β/γ
Laminin
Protein Level
(Relative to Laminin)
P < 0.005
P < 0.005
1.00 ± 0.18
0.21 ± 0.10
1.00 ± 0.26
0.04 ± 0.02
WT KO WT KO
COL4A1 COL4A2
C
kDa
WT KO WT KO WT KO COL4
238
171
COL4A1
238
171
COL4A2
62
49
β tubulin
Protein Level
(Relative to β tubulin)
P < 0.001
6.30 ± 0.81
P = 0.17
1.00 ± 0.24
1.00 ± 0.25
0.75 ± 0.08
WT KO WT KO
COL4A1 COL4A2
D
(min) 30 60 90 120 150 180 210 240 270 300 360 420 480 ctrl
Alexa 448 - AHA
Time (min)
E
WT KO WT KO
(h) 8 8 24 48 8 8 24 48
Alexa 448 - AHA
0.03 ± 0.01
0.13 ± 0.03
0.24 ± 0.13
8h 8h 24h 48h
WT KO

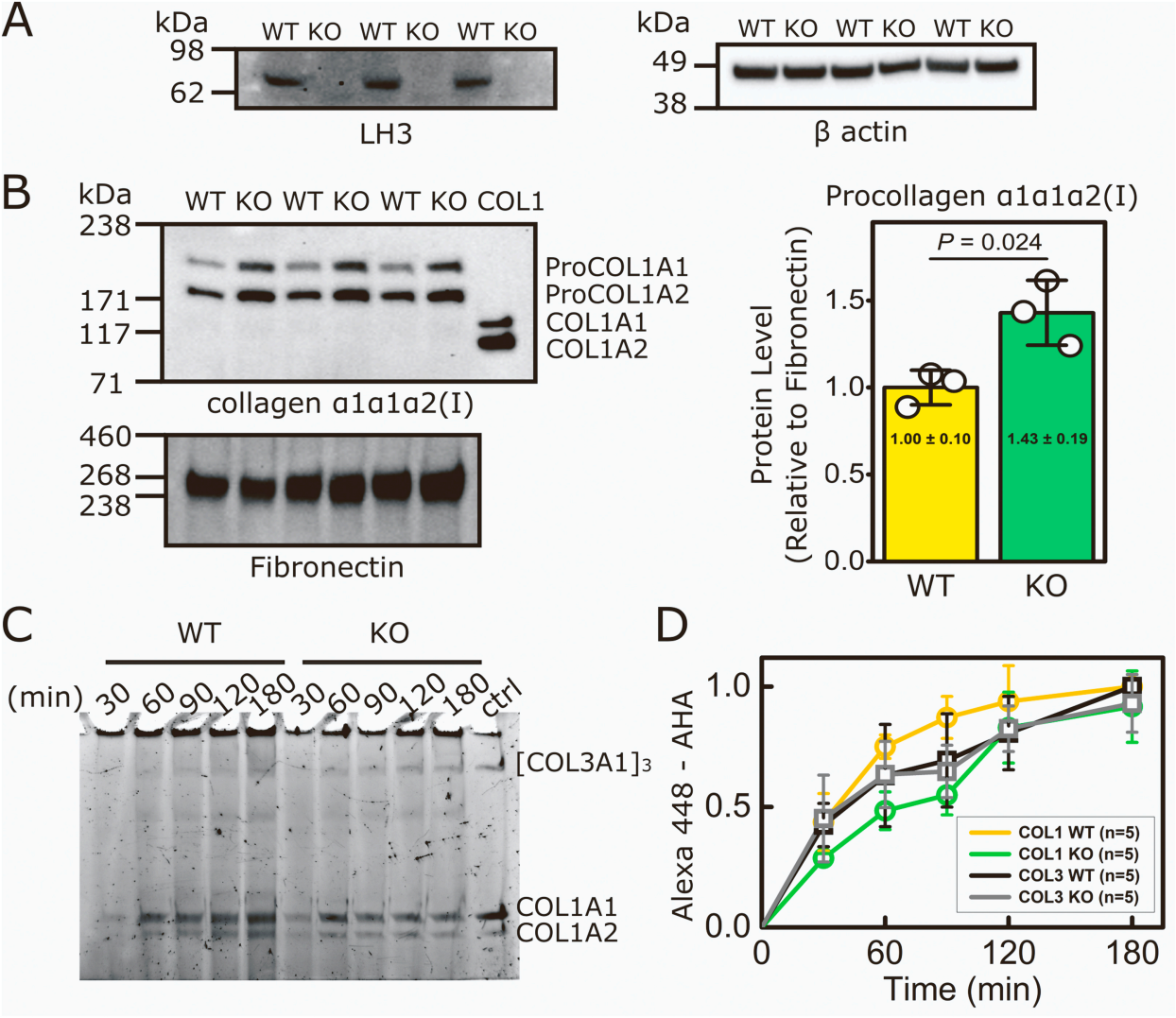
A
kDa
98
62
WT KO WT KO WT KO
LH3
kDa
49
38
WT KO WT KO WT KO
β actin
B
kDa
238
171
117
71
WT KO WT KO WT KO COL1
ProCOL1A1
ProCOL1A2
COL1A1
COL1A2
collagen α1α1α2(I)
460
268
238
Fibronectin
Procollagen α1α1α2(I)
P = 0.024
Protein Level
(Relative to Fibronectin)
1.5
1.0
0.5
0.0
1.00 ± 0.10
1.43 ± 0.19
WT
KO
C
WT
KO
(min)
30
60
90
120
180
30
60
90
120
180
ctrl
[COL3A1]3
COL1A1
COL1A2
D
Alexa 448 - AHA
1.0
0.5
0.0
0
60
120
180
Time (min)
COL1 WT (n=5)
COL1 KO (n=5)
COL3 WT (n=5)
COL3 KO (n=5)

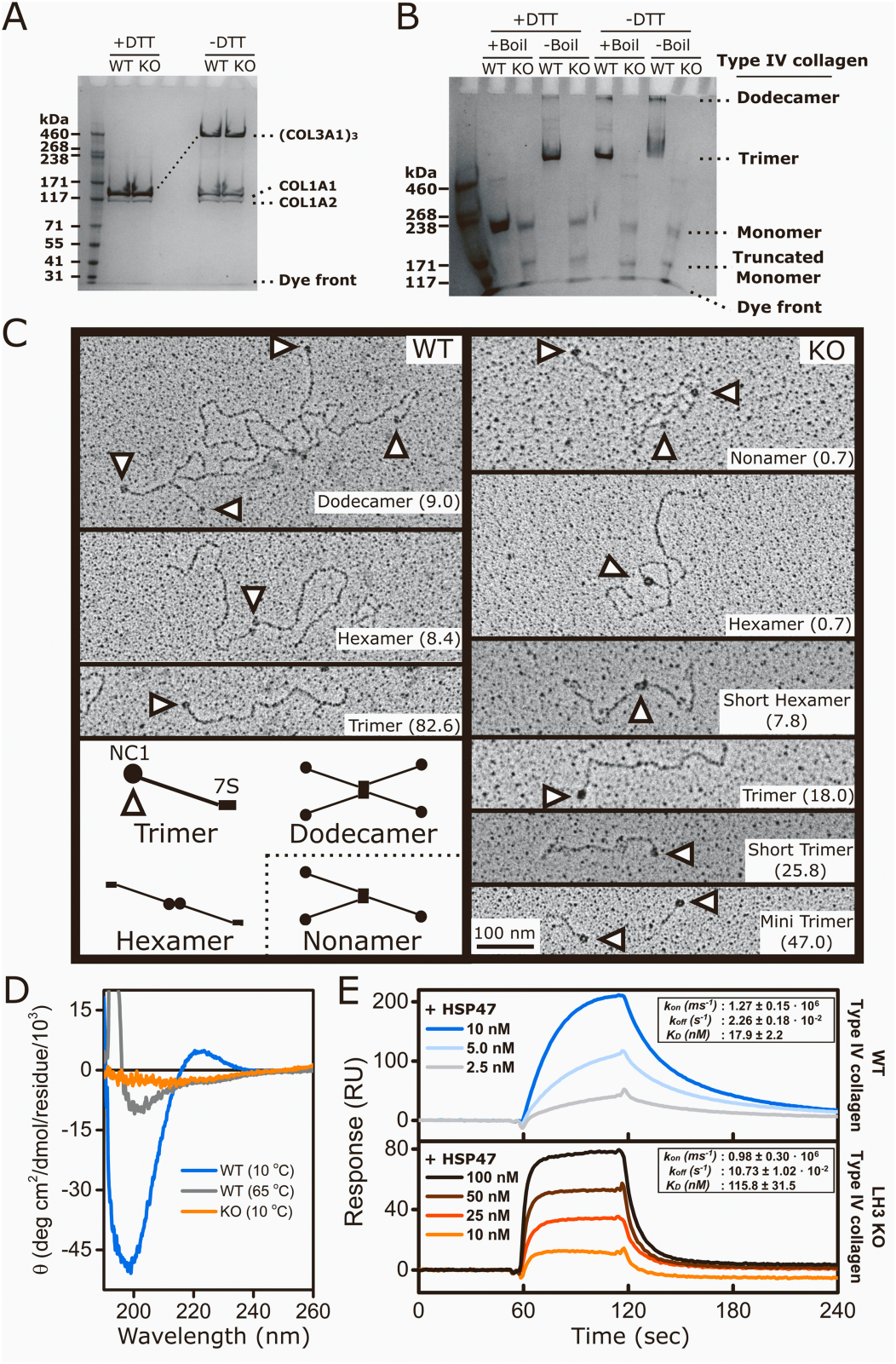
A
+DTT
-DTT
WT KO
WT KO
kDa
460
268
238
171
117
71
55
41
31
(COL3A1)3
COL1A1
COL1A2
Dye front
B
+DTT
-DTT
+Boil
-Boil
+Boil
-Boil
WT KO WT KO WT KO WT KO
Type IV collagen
kDa
460
268
238
171
117
Dodecamer
Trimer
Monomer
Truncated Monomer
Dye front
C
WT
KO
Dodecamer (9.0)
Hexamer (8.4)
Trimer (82.6)
Nonamer (0.7)
Hexamer (0.7)
Short Hexamer (7.8)
Trimer (18.0)
Short Trimer (25.8)
Mini Trimer (47.0)
NC1
7S
Trimer
Dodecamer
Hexamer
Nonamer
100 nm
D
θ (deg cm2/dmol/residue/10^3)
15
0
-15
-30
-45
WT (10 °C)
WT (65 °C)
KO (10 °C)
200
220
240
260
Wavelength (nm)
E
+ HSP47
10 nM
5.0 nM
2.5 nM
kon (ms-1) : 1.27 ± 0.15 · 10^6
koff (s-1) : 2.26 ± 0.18 · 10^-2
KD (nM) : 17.9 ± 2.2
WT Type IV collagen
+ HSP47
100 nM
50 nM
25 nM
10 nM
kon (ms-1) : 0.98 ± 0.30 · 10^6
koff (s-1) : 10.73 ± 1.02 · 10^-2
KD (nM) : 115.8 ± 31.5
LH3 KO Type IV collagen
Response (RU)
200
100
0
80
40
0
60
120
180
240
Time (sec)

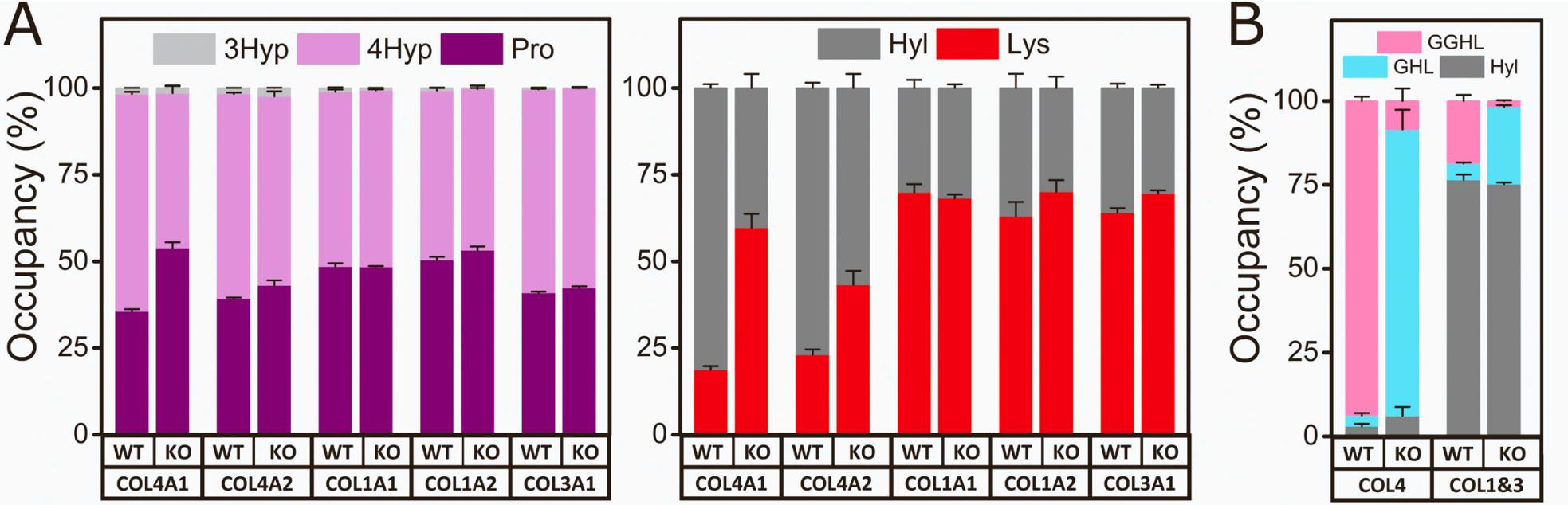
A
3Hyp
4Hyp
Pro
Occupancy (%)
100
75
50
25
0
WT
KO
COL4A1
COL4A2
COL1A1
COL1A2
COL3A1
Hyl
Lys
B
GGHL
GHL
Hyl
COL4
COL1&3

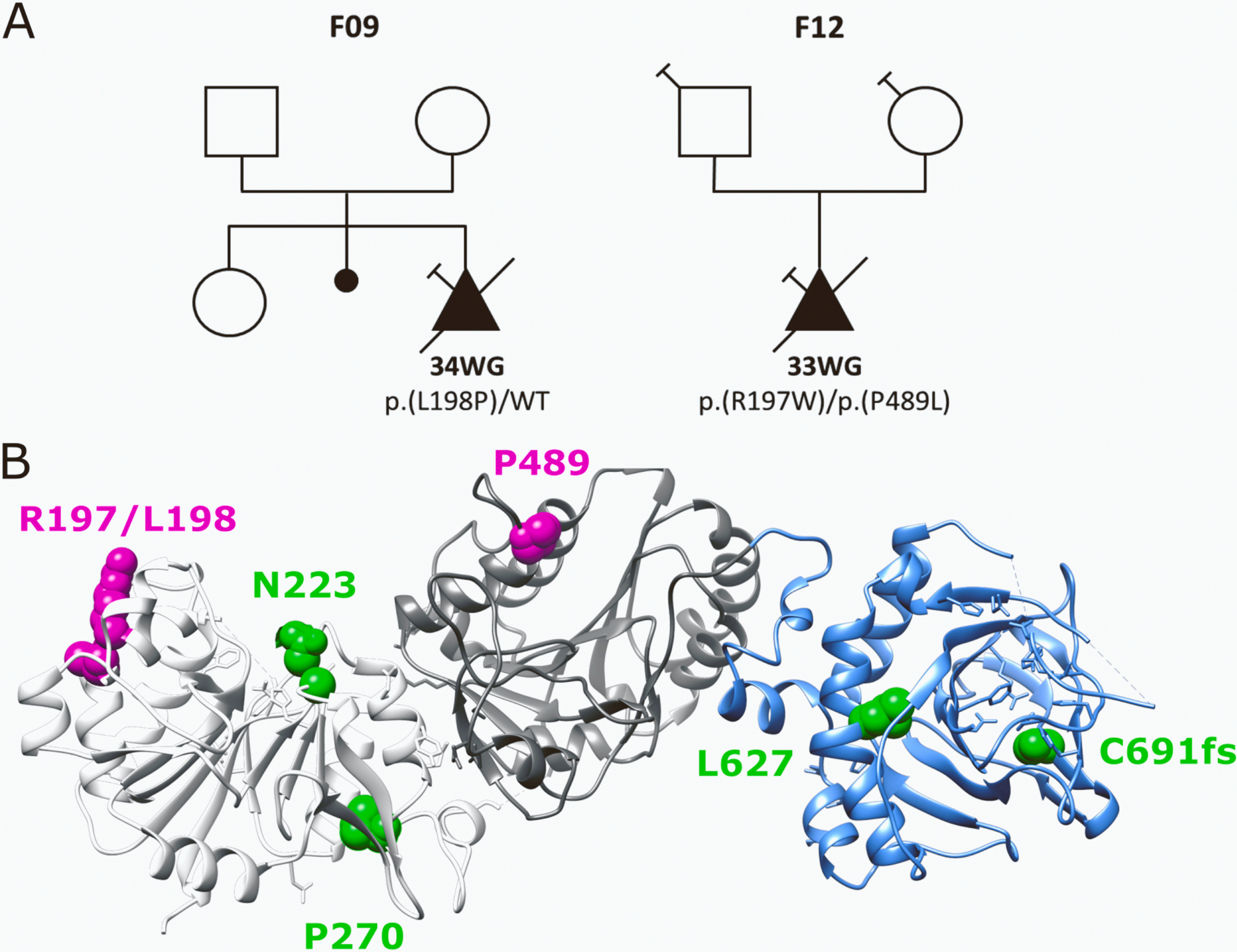
A
F09
F12
34WG
p.(L198P)/WT
33WG
p.(R197W)/p.(P489L)
B
P489
R197/L198
N223
L627
C691fs
P270

Yoshihiro Ishikawa: Conceptualization, Methodology, Validation, Formal analysis, Investigation, Resources, Data Curation, Writing - Original Draft, Writing - Review & Editing, Visualization, Supervision, Project administration, Funding acquisition

Yuki Taga:, Methodology, Validation, Formal analysis, Investigation, Data Curation, Writing - Review & Editing

Thibault Coste: Validation, Formal analysis, Investigation, Resources, Data Curation, Writing - Review & Editing

Sara F. Tufa: Methodology, Validation, Formal analysis, Investigation, Data Curation, Writing - Review & Editing

Douglas R. Keene: Methodology, Validation, Formal analysis, Investigation, Data Curation, Writing - Review & Editing

Kazunori Mizuno: Data Curation, Writing - Review & Editing

Elisabeth Tournier-Lasserve: Conceptualization, Data Curation, Writing - Review & Editing, Supervision, Project administration

Douglas B. Gould: Conceptualization, Data Curation, Writing - Original Draft, Writing - Review & Editing, Supervision, Project administration, Funding acquisition